ELECTRONIC PROPERTIES OF NBS_2 SINGLE LAYERS

by

ZHANMING LI

B.Sc., Zhongshan University, 1982

A THESIS SUBMITTED IN PARTIAL FULFILMENT OF

THE REQUIREMENTS FOR THE DEGREE OF

MASTER OF SCIENCE

in

THE FACULTY OF GRADUATE STUDIES

Department Of Physics

We accept this thesis as conforming

to the required standard

THE UNIVERSITY OF BRITISH COLUMBIA

Sept. 1984

© Zhanming Li, 1984

In presenting this thesis in partial fulfilment of the requirements for an advanced degree at the University of British Columbia, I agree that the Library shall make it freely available for reference and study. I further agree that permission for extensive copying of this thesis for scholarly purposes may be granted by the head of my department or by his or her representatives. It is understood that copying or publication of this thesis for financial gain shall not be allowed without my written permission.

Department of Physics

The University of British Columbia
1956 Main Mall
Vancouver, Canada
V6T 1Y3

Date Oct. 15, 1984

DE-6 (3/81)

Abstract

A theory of optically and magnetically anisotropic NbS_2 platelets suspended in water is developed, and a two dimensional tight-binding model is used to describe the magnetic and optical properties of single layer NbS_2 and $NbSe_2$. For the first time both polarization and transition matrix effects are included in calculating the intensities of absorption of the transition metal dichalcogenides. The results are in qualitative agreement with experiments and can be interpreted in terms of the two dimensional(2D) nature of the band structure.

Table of Contents

List of Tables

List of Figures

Acknowledgement

I am obliged to my advisor, Professor B. Bergersen who has initiated this work and given valuable advice throughout its completion.

Mr. C. Liu and Dr. R.F.Frindt have kindly provided details and data of the experiment.

I have benefited from the inspiring conversations with Dr. P.Palffy-Muhoray on the ratio of the obsorption intensities.

Thanks also go to Dr. S. Sharma for her helpful information provided during the computer programing of the band structure calculation.

The financial support from the University of British Columbia is gratefully acknowledged.

I. INTRODUCTION

The transition metal dichalcogenides (TMD's) have been the object of a great deal of recent study due to the observation of charge density waves (CDW's) with associated periodic lattices distortions[1]. Two models are proposed for the formation of CDW's[2,3]. Since both of them are based on the quasi-2D nature of the compounds, it will be of experimental and theoretical interests to study the properties of single layer TMD's. The recent succssful preparation of single layer NbS_2 [4,17,19] motivate us to study the electronic properties of the compounds using a 2D model.

Although no CDW's are observed in the single layers, a theoretical study will help one to understand to what extent the TMD's are two dimensional. In both the experiment and this work one finds considerable enhancement of magnetic susceptibilities in the single layer compounds, which is related to the recent observations of the magnetic properties of thin films, surfaces and interfaces[5]; therefore the magnetic behavior of the compounds is interesting in its own right.

After a brief introduction to the structure and properties of the TMD's and the recent experiment results on single layer NbS_2 in this chapter ,we will analyse the experiment results with a simple model in chapter 2, and we present a tight binding calculation as modified from that of Doran et.al.[6] in chapter 3. Finally we will use the tight binding model to calculate the magnetic and optical properties of the compounds.

A. STRUCTURE AND PROPERTIES OF THE 2H-TMD

The materials 2H-NbS_2 and 2H-$NbSe_2$ belong to the family of layer transition metal dichalcogenides (from group IVB, V and VIB) as reviewed by Wilson and Yoffee[7]. The structure of both compounds consists of molecular sandwiches with one sheet of transition metal atoms between two sheets of chalcogen atoms. The crystal has two sandwiches in a unit cell with the atoms in each sandwich forming a triangular lattice. To establish our coordinate system and notation we illustrate the structure schematically in FIGURE 1. The crystallographic data are listed in TABLE 1.

*Crystallographic data (in atomic units)[7,10] used in our calculation. a, separation within a monolayer; w, height of Van der Waals gap; s, height of sandwich.

	a	s	w
2H-NbS_2	6.26	5.94	5.29
2H-$NbSe_2$	6.50	6.31	5.48

Table I - Crystallographic data

Due to the weak interlayer interation, the anisotropies in electric conductivity is very large. For example, in metallic

compounds, the conductivity parallel to the layer can be as large as 50 times that perpendicular to the layer. The most interesting feature of TMD's, however, is that many of them exhibit a transition to both CDW states and superconducting states at low temperatures.

There have been two popular models for the CDW transitions, the nesting model and the saddle point model. In the nesting model[2] , parallel sections of Fermi surfaces that are spanned by a wave vector $\vec{q}$, give rise to a divergent electric susceptibility, χ^e.

$$\chi^e = \sum_{\vec{k}} (n(\vec{k})(1-n(\vec{k}))/(E(\vec{k})-E(\vec{k}+\vec{q})) \qquad (1.1)$$

where $n(\vec{k})$ is the Fermi funtion. In the saddle point model[3], two saddle points on the Fermi surface spanned by a wave vector q lead to the divergence of (1.1). Clearly both of the models are based on the geometry of the quasi-2D band structure.

B. A RECENT EXPERIMENT

We will next discuss some experiment results[4,19] as the motivation for this work. In the experiment, single layer platelets of NbS_2 freely suspended in water have been prepared using a technique involving intercalation of hydrogen and water, and the single layer structure has been determined by X-ray diffraction experiment. Since the sample is homogeneous one can perform optical absortion experiment on it. For the convevience of later reference, the optical absorption spectra (plotted as ln(Io/I),where Io is the intensity of the incident light) of

single layer NbS_2 are reproduced in FIGURE 2[4].

Compared to the absorption spectra of the 3D single crystal, the spectra of the platelets have the same main absorption peak at 2.7 eV, but a considerable reduction at lower frequencies is observed. The reduction can be explained in terms of the increase in band gap between p/d bands (bands arising from p orbitals in the language of tight binding method) and the dz^2 band as will be shown in chapter 3.

Due to the anisotropy in magnetic susceptibilies,one can align the platelets with a strong magnetic field(see FIGURE 3). The anisotropy in optical properties then enables one to use polarized light to study the polarization effect on the absorption spectra. The polarization dependent absorption intensities at 4600 Angstrom are shown in FIGURE 4. To understand the spectra and the polarization effect, which is the goal of this work, one needs a theory of band structure as well as a macroscopic model for the statistical behavior of the platelets suspended in water.

II. THEORY OF ANISOTROPIC PLATELETS IN WATER

A. A MACROSCOPIC MODEL

For a continuous medium with optical absorption coefficient, a, the intensity has the following forms:

$$dI=-aI.dt \qquad (2.1)$$

$$I=I_0\exp(-at) \qquad (2.2)$$

where I is the intensity of light and t is the length of the path through the medium.

Consider a distribution of platelets with mean volume V_0 and let $P_2(v)$ be the propability that a given platelet has a volume $V=vV_0$. We assume that

1) the whole system can be considered as a continuous medium.

2) macroscopic scattering is negligible.

3) demagnetization and electrostatic effects are negligible.

We can derive similar relations for the two cases when the polarization vecter , $\underset{\rightarrow}{E}$, is parallel and perpendicular to the applied magnetic field, $\underset{\rightarrow}{B}$, respectively:

Case 1. $\underset{\rightarrow}{E}$ parallel to $\underset{\rightarrow}{B}$

$$-dI/Idt=\int\int v(a_3\cos^2\theta+a_1\sin^2\theta)P_1(v,\Omega)\ P_2(v)d\Omega dv \qquad (2.3)$$

Here a_1 and a_3 are the absorption coefficients corresponding to polarizations parallel and perpendicular to the plane respectively, and $\Omega = (\theta, \varphi)$ are the polar angles defined in FIGURE 5, and $P_1(v,\Omega)d\Omega$ is the conditional probability of finding a platelet within $d\Omega$ when the volume is v.

Case 2. E perpendicular to B

$$-dI/Idt=\int\int v[a_3\cos^2\varphi\sin^2\theta+a_1(\sin^2\varphi+\cos^2\varphi\cos^2\theta)]P_1(v,\Omega)P_2(v)d\Omega dv \qquad (2.4)$$

The interaction energy can be written as

$$H=-VB^2[\chi_1+(\chi_3-\chi_1)\cos^2\theta]/\mu_0 \qquad (2.5)$$

Thus we have

$$P_1(v,\Omega)=\exp(-H/kT)/\int\exp(H/kT)d\Omega \qquad (2.6)$$

where χ_1 and χ_3 are the magnetic susceptibilities parallel and perpendicular to the plane respectively.

For the size distribution we choose

$$P_2(v)=\exp(-v) \qquad (v>0) \qquad (2.7)$$

for the following reasons. It truncates at zero and has a tail towards $v=\infty$, and its standard deviation is in reasonable agreement with the experimental observations[4] that size ranges from about 50nm to 300nm. It is simple mathematically. And most important of all is that it fits the experiment curve better than the other distributions such as normal and vexp(-v)

distributions when we use a least square fit method. Integrating (2.3) and (2.4) over $d\Omega$,dv and dt gives

$$I_{30}/I_3=\exp\{[a_1-(a_1-a_3)\ \langle v\cos^2\theta\rangle]t\} \qquad (2.8)$$

$$I_{10}/I_1=\exp\{0.5[a_3+a_1+(a_1\ -a_3)\langle v\cos^2\theta\rangle]t\} \qquad (2.9)$$

$$\langle v\cos^2\theta\rangle=\int v\cos^2\theta\, P_1P_2 d\Omega dv \qquad (2.10)$$

where I_3 and I_1 are the absorption intensities with $\underline{E}$ parallel and perpendicular to the magnetic field respectively, and I_{30} and I_{10} are the corresponding intensities of the incident light. < > here means average over Ω and v. (2.8) and (2,9) are the results of our model to be fitted to the experiment data.

B. FITTING THE MODEL TO THE EXPERIMENT

If one chooses a_1t,and a_3t in (2.8,9) and $(\chi_3-\chi_1)$ as parameters to be fitted to the experiment curve in reference 4, one is able to plot I_{10}/I_1 and I_{30}/I_3 as funtions of B,as is illustrated in FIGURE 4. The value of quantities in the fitting and the results of the three parameters are shown in TABLE 2.

Compared to the published data shown in TABLE 3, where we have converted the original emu/g unit into the cgs dimensionless unit, one finds that the anisotropies of the single layer NbS_2 are a few times larger than those of many of the 3D TMD crystals. This value is inversely proportioal to the assumed mean value of the platelets. The value given in TABLE 2 was suggested to us by C. Liu based on electromicroscope observations[4].

$V(M^3/10^{23})$	2.4
$kT(J/10^{21})$	4.04
a_1t	3.34
a_3t	0.81
$\chi_3-\chi_1(cgs/10^6)$	26

Table II - Data of the fitting for NbS_2

	$NbSe_2$	TaS_2	$TaSe_2$
χ_3*	8.8	8.4	9
χ_1*	4.8	4.2	3.6

*χ's are all in $cgs/10^6$[14][18]

Table III - Experimental data of magnetic susceptibility of TMD

We comment here that probably because of light scattering, there is some descrepancy in the ratio of the absorption intensities(see equation(2.12)). If one fits each curve separately , one obtains slightly different parameters, and the $\chi_3-\chi_1$ in TABLE 4 is the average of the two fits.

Although experiments are lacking for data of single crystal NbS_2, we can still make the comparision because,from TABLE 3. the anisotropic susceptibilities are about the same for all 2H-

TMD's and in agreement with the calculation of McDonald and Geldart[14].

To see how the platelets order under the magnetic field we also plot the order parameter[8],S

$$S=0.5(3\langle\cos^2\theta\rangle-1) \qquad (2.11)$$

vs the magnetic field in FIGURE 4. From the plot one sees that the alignment of the platelets reaches its saturation value at about 50 kGauss.

To examine the validity of the theory, we plot

$$R=\ln(I(0)/I_1)/\ln(I_3/I(0)) \qquad (2.12)$$

in FIGURE 7 according to the digitized data from experiment curve in FIGURE 6, where I(0) is the intensity when B=0. It is found that R is colour dependent and not always equal to 2 as the theory predicts (see (2.8,2.9)). The R value(=2.6) at the absorption peak explains the deviation of theory from the experiment. We believe that the large deviation of R from 2 in frequencies away from the absorption peak is due to light scattering. In those frequencies absorption in both polarizations is so small that the extintion of intensity is dominated by scattering light. At low frequencies, scattering in the polariztion parallel to the plane of the platelets is larger than that in the other direction, and the inverse situation applies to the high frequencies.

III. FERMI SURFACES AND BAND STRUCTURES OF THE SINGLE LAYERS

Among the 2H family of TMD's, NbS_2 has received less attention than the others partly because it is difficult to make good specimens, and partly because it appears to be less remarkable than the other member of the family. CDW which has been observed in the other compounds[1] at low temperatures is inhibited in NbS_2 , perhaps totally. As the first attempt to study the differences in electronic structure between NbS_2 and the other compounds, Wexler and Woolly(1975)[9] calculated the band structures of $TaSe_2$,TaS_2,$NbSe_2$ and NbS_2 using a layer method and a similar potential to that of Matheiss[10]. They found some differences which seemed to be determined by the chalcogen rather than the metal.

A. A TIGHT BINDING FIT TO THE BANDS OF THE 2H-TMD

To calculate numerically $\overset{e}{\chi}(q)$, the electric susceptibility which play a decisive role in the occurrence of CDW, Doran et.al. [6,11] used a Slater-Koster tight binding fitting scheme[12] to fit their Hamiltonian to the band structure calculation of Wexsler and Woolly[9]. To establish notations and facilitate comparision we describe below their results briefly.

2H-NbS_2 (and 2H-$NbSe_2$) has D_{6h}^4 space group symmetry. A unit cell is shown in FIGURE 1(b). Following the notations of ref.6, a Bloch sum over N lattice sites in the crystal is given by

$$|\psi\rangle = N^{-1/2}\exp[i\vec{k}.(\vec{R}+\vec{d})]|a(\vec{r}-\vec{R}-\vec{d})\rangle \qquad (3.1)$$

$\vec{d}$ is a vector from the origin to atoms in the unit cell, and the $|a\rangle$'s are the symmetric and antisymmetric combination of the atomic orbitals belonging to the same sandwich. That is

$$|X_{-1}\rangle = |X(\text{site}1)\rangle - |X(\text{site}3)\rangle$$
$$|X_{-2}\rangle = |X(\text{site}4)\rangle + |X(\text{site}6)\rangle$$
$$\text{etc.} \qquad (3.2)$$

In this way the Bloch sums are divided into even and odd funtions with respect to the plane of the sandwich. With this choice of the basis the Hamiltonian matrix can be written schematically as:

Sandwich		1		2	
		Even	Odd	Even	Odd
1	Even	A(6x6)	0	Ccos(Sz)	Esin(Sz)
	Odd	0	B(5x5)	$-E^{T}\sin(Sz)$	Dcos(Sz)
2	Even	$C^{*T}\cos(Sz)$	$-E^{*}\sin(Sz)$	A^{*}	0
	Odd	$E^{*T}\sin(Sz)$	$D^{*T}\sin(Sz)$	0	B^{*}

where Sz=0.5cK (c=2(w+s)), and the matrix elements are expressed in terms of the energy integral of Slater and Koster[12] which

are in turn written in terms of the two-centre parameters. It is these latter parameters which are used in the fitting procedure.

The results of the fitting are given in FIGURES 8 , 9 and 10, where the symmetry points are indicated in FIGURE 11. The band structure is charaterized by an isolated dz^2 band between the upper d-bands and the lower p-bands and a Fermi surface well above the saddle points[9].

B. BAND STRUCTURE OF SINGLE LAYERS

To apply the tight binding fit to the single layer compounds, we modify the fit by setting the interlayer interaction to zero,that is, by setting C,D and E matrices to zero. The modified bands and the Fermi surfaces are shown in FIGURES 12,13 ; 14,15 respectively, Shown in FIGURE 16 are the densities of states of dz^2 bands which are calculated by a 2D analog of the tetrahedron method[13]. The detailed formulas in the method are worked out in Appendix C. In the calculation we have generated a grid with 1600 triangles in an irreducible Brillouin zone as shown in FIGURE 17(a) .

The atomic orbitals and their angular part in one sandwich are numbered in the way described in TABLE 4.

The main features of the 2D and 3D bands are essentially the same except a 0.5 eV increase in the band gap from p/d to dz^2 which will affect the interband transitions as will be shown in chapter 5. One also notes that the energy dispersions along MK and ALHA are exactly the same as they should. Moreover, FIGURE 16 shows that the reduction of the third dimension gives

rise to high density of states, especially in NbS_2. The reason why the density of states of single layers of $NbSe_2$ is lower than that of NbS_2 is that the saddle points are less pronounced in $NbSe_2$ as can be seen from FIGURES 14 and 15.

From Figure 14 , one sees that besides the well known saddle point between ΓP, a new saddle point arises between QP as a consequence of the 2D model, which leads to the peak around the Fermi energy. Mathematically, due to the saddle points the density of states will diverge logarithmically, but in computations one hardly get any divergence due to the limit set by the computational method . Therefore one must be careful if the Fermi surface lies at the saddle point.

even			odd		
orbitals	number	ang.fn	orbitals	number	ang.fn
$3z^2-r^2$	1	Y_2^0	xz	1	$(Y_2^1+Y_2^1)/\sqrt{2}$
x^2-y^2	2	$(Y_2^2+Y_2^{-2})/\sqrt{2}$	yz	2	$(Y_2^1-Y_2^{-1})/\sqrt{2}i$
xy	3	$(Y_2^2-Y_2^{-2})/\sqrt{2}i$	x-	3	$(Y_1^1+Y_1^{-1})/\sqrt{2}$
x+	4	$(Y_1^1+Y_1^{-1})/\sqrt{2}$	y-	4	$(Y_1^1-Y_1^{-1})/\sqrt{2}i$
y+	5	$(Y_1^1-Y_1^{-1})/\sqrt{2}i$	z+	5	Y_1^0
z-	6	Y_1^0			

Table IV - Atomic orbitals used in the tight binding fit

IV. MAGNETIC SUSCEPTIBILITY OF SINGLE LAYER COMPOUNDS

Although energy band structures of metallic TMD's have been calculated and studied by many authors[1,7,6,9,10], the magnetic susceptibility, χ, was seldom calculated by theory due to the complicated electronic structure of the compounds[14]. To estimate the anisotropic magnetic susceptibility of the single layers which is measured indirectly from the optical absorption experiment (as was shown in chapter 2.), we adopt the 2D tight-binding Hamiltonian as was shown in last chapter.

In considering the susceptibility based on the 2D model, we follow the development of Misra and Kleiman[15](for the application of the theory in our case see Appendix A). Because of the high density of states, we expect the Pauli susceptibility to dominate and ignore contributions from other sources, and write

$$\chi = -\sum_{\vec{k}} \frac{\mu_B^2}{2} (g_{n,\vec{k}}^{\vec{\alpha}})^2 f'(E_n(\vec{k})) \qquad (4.1)$$

where E_n is the Bloch eigenvalue in the absence of the field, $\vec{\alpha}$ is in the diretion of the field, and

$$(g^{\bar{\alpha}}_{n\bar{k}})^2=4(|\langle n,\vec{k},+|\mu_{\bar{\alpha}}|n,\vec{k},+\rangle|^2+|\langle n,\vec{k},+|\mu_{\bar{\alpha}}|n,\vec{k},-\rangle|^2) \qquad (4.2)$$

where $|n,k,+(-)\rangle$ is one of the Kramer degenerate states with wave vector $\vec{k}$ and band label n and $\vec{\mu}$ is the periodic part of the magnetic moment operator[15]. In the tight binding limit, the simplest appproximation is to write

$$\langle n,\vec{k},s|\mu_{\bar{\alpha}}|n,\vec{k},s'\rangle=\langle n,\vec{k}|L_{\bar{\alpha}}|n',\bar{k}\rangle\delta_{\sigma\sigma'}+\delta_{n,n'}\langle\sigma|\sigma_{\alpha}|\sigma'\rangle \qquad (4.3)$$

where $\langle n,\bar{k}|L_{\bar{\alpha}}|n',\bar{k}\rangle$ is the matrix element of the orbital angular momentum operator between the angular parts of the tight-binding basis funtions and $\langle\sigma|\sigma_{\alpha}|\sigma\rangle$ is the Pauli spin matrix element(see Appendix B) . In writing (4.2), we negleted the interband matrix element due to the large band gap between dz^2 band and other bands. The above aproximation method is in the same spirit as McDonald and Geldart[14].

In evaluating (4.2), we have taken the advantage of the 2D nature of the electronic structure by using a 2D tetrahedron method mentioned in chapter 3. The eigenvalues and eigenvetors of the tight binding Hamiltonian are obtained by using standard matrix techniques(by calling a subroutine EIGZC from the IMSL library) to diagonalize the Hamiltonian matrix.

(4.2) is then evaluated at each $\bar{k}$ point in our Brillouin zone grid (see FIGURE 17.) by using (4.3) and the wave funtion obtained in the program. We find that

$$\langle g^{z\,2}\rangle/\langle g^{x\,2}\rangle\approx 4 \qquad (4.4)$$

where < > means average over the Brilloun zone. We interpret this result in a simple model as follows. First consider the ligand field model by setting H , the periodic potential to zero. Then the splitting of d-orbitals under D_{3h} point group is simplly dz^2,(x^2-y^2,xy), and (zx,yz) in ascending order[10]. Since the Fermi surface lies in the second level, we have a state |2,±2>. When a magnetic field is applied to the system, the splitting of |2,±2> gives

$$g = 2\langle 2,+2|Lz|2,+2\rangle + 2 = 6$$

$$g = 2\langle 2,+2|Lx|2,+2\rangle + 2 = 2 \qquad (4.5)$$

When the periodic potential is turned on, the intraatomic interactions quench the orbital contributions to g and we get (4.4)

The results obtained for $\chi(T=0)$ and D(E), the density of states are shown in TABLE 5.

Considering the uncertainty in the partical size distribution, the agreement between theory and experiment is quite satisfactory. One also notes that the density of states in the 2D model is considerablly larger than in 3D (see FIGURE 16) mainly because in 2D there is no dispersion of energy in the z direction.

	NbS_2	$NbSe_2$
D*	35	22
χ_1	4.9	3.2
χ_3	24	16
$\chi_3-\chi_1$	19	13
$\chi_3-\chi_1^{exp}$	26	

*In the table the unit of D is 1/(Ryd.Nb.spin); the unit of χ is cgs/10^6.

Table V - Magnetic susceptibilities from the theory

V. OPTICAL PROPERTIES OF THE SINGLE LAYER COMPOUNDS

To understand the absorption spectra arising from the interband transitions one needs to calculate the joint density of states and the oscillator strength. In the case of single layers of NbS_2 and $NbSe_2$, the tight binding matrix block diagonalizes and the energy bands separate into σ and π bands as indicated in FIGURE 18 and 19 respectively. For transitions below 5 eV, we only consider the transitions from p/d bands to dz^2 band because transitions from d-orbitals to d-orbitals are forbiden and d/p bands are dominated by d-orbitals(the evidence of which is shown in FIGURE 20).

We believe that the following calculation is the first attempt to include both the polarization and the matrix element effect when considering optical transitions in a solid.

The optical joint density of states funtion can be written as

$$J(E) \sim \int dS / \nabla_{\vec{k}}(E_V - E_C) \qquad (5.1)$$

where E_C and E_V are the energy eigenvalues of the conduction band and valence band respectively. Since we are considering direct interband transitions, care has been taken to avoid counting transitions from p/d band to the occupied portion of the dz^2 band. The results obtained by the tetrahedron method mentioned earlier for σ-to-σ and π-to-π transitions are shown in FIGURES 21 and 22 respectively.

From FIGURE 21, one notes that there is no interband

transition below 2.5 eV which acounts for the reduction of absorption in low frequency region (see FIGURE 2). One also finds that both σ-to-σ and π-to-π transitions have a peak at 2.7 eV as was observed in the experiment(see FIGURE 2.) . But the magnitude of density funtion for π-to-σ transition is about twice as large as that for σ-to-σ transition, while the experiment gaves $a_1=4a_3$(see ref.4 and TABLE 5). To account for the experiment results one needs to consider the oscillator strength or the transition matrix

$$F_{cv}=2mE_{cv}|r_{cv}|^2/\hbar=2\hbar|\nabla_{vc}|^2/mE_{vc} \qquad (5.2)$$

where

$$r_{vc}=\langle\psi_v|r|\psi_c\rangle$$
$$\nabla_{vc}=\langle\psi_v|\nabla_i|\psi_c\rangle \qquad (5.3)$$

and

$$|\psi_v\rangle=\sum_i v_i|i\rangle$$
$$|\psi_c\rangle=\sum_i c_i|i\rangle \qquad (5.4)$$

are the wave funtions of the valence and conduction bands respectively with $|i\rangle$ being the bloch sum for the ith atomic orbital.

We consider transitions from σ to σ first. In order to evaluate $\langle\psi_v|r|\psi_c\rangle$ in the tight binding limit, one needs to calculate terms like

$$\langle Y_l^{m'}(\theta',\varphi')g(|\vec{r}-\vec{R}|)|\vec{r}|Y_l^{m}(\theta,\varphi)f(r)\rangle\exp\{iP_1(\vec{k},\vec{R})-iP_2(\vec{k},\vec{R})\} \qquad (5.5)$$

where θ' and φ' are funtions of θ, φ and $\vec{r}$, and $\exp\{iP_1(\bar{k},\bar{R})\}$ and $\exp\{iP_2(\bar{k},\bar{R})\}$ are the phase factors that give the correct linear combinations of atomic orbitals when combined with V_i's and C_i's respectively. Since a $\vec{k}$ and $\bar{d}$ dependent factor is included in the original Bloch sums[6], the funtion $P(\bar{k},\bar{d})=P_1-P_2$ is rather complicated.

We make the following approximations for the z component.

$$
\begin{aligned}
&\langle Y_{l'}^{m'}(\theta',\varphi')g(|\bar{r}-\bar{R}|)|\cos\theta r|Y_l^m(\theta,\varphi)f(r)\rangle\exp\{iP(\vec{k},\vec{R})\}\\
&\approx\langle Y_{l'}^{m'}(\theta',\varphi')|\cos\theta r^0|Y_l^m(\theta,\varphi)\rangle\langle g(|\bar{r}-\bar{R}|)|\ f(r)\rangle\exp\{iP(\bar{k},\bar{R})\}\\
&\approx\langle Y_{l'}^{m'}(\theta,\varphi)|\cos\theta r^0|Y_l^m(\theta,\varphi)\rangle\langle g(|\bar{r}-\bar{R}|)|\ f(r)\rangle\exp\{iP(\bar{k},\bar{R})\}
\end{aligned}
\tag{5.6}
$$

and similarly for the x and y componet,

where r^0 is some constant of the order of the lattice spacing, and the second step of the approximation treats the anglar parts of the atomic orbitals as if they were on the same site.

After substituting (5.6) into (5.3), we make the further approximation:

$$
\begin{aligned}
&\langle g(|\bar{r}-\bar{R}|)|\ f(r)\rangle\exp\{iP(\bar{k},\bar{R})\}\\
&\approx S_{ij}(\bar{k})\\
&=\langle Y_{l'}^{m'}(\theta',\varphi')g(|\bar{r}-\bar{R}|)|Y_l^m(\theta,\varphi)f(r)\rangle\exp\{iP(\bar{k},\bar{R})\}
\end{aligned}
\tag{5.7}
$$

where S_{ij}'s are the overlap matrix elements generated from the computer program. This step is needed because $S_{ij}(\bar{k})$'s take care of the phase factor. The above three steps of approximation enable one to make use of the V_i's,C_i's and $S_{ij}(\bar{k})$'s from the

program and of the well-known selection rules in atomic physics. Then

$$\begin{aligned} &\langle \Psi_v | r | \Psi_c \rangle \\ &= V_i^*(\bar{k}) C_j(\bar{k}) T_{ij} S_{ij}(\bar{k}) \end{aligned} \qquad (5.8)$$

where T_{ij}'s are the r matrix element between the anglar part of the atomic orbitals(the atomic transition matrices) as worked out in Appendix D.

In the case of π to σ transition S_{ij}'s are zero, and one has to modify the above approximation method. In Appendix D. we note that there are only three nonzero T_{ij}'s and only one of them is large, i.e. ,corresponding to transition from p to d-orbitals. Therefore the phase factor exp{iP} is not important and one can still use the nonzero S_{ij}'s corresponding to the σ-to-σ transition to estimate the π-to-σ transition. Averaging (5.8) over the Brillouin zone gives

$$|\langle \Psi_v | x | \Psi_c \rangle|^2 / |\langle \Psi_v | z | \Psi_c \rangle|^2 = 6.9 \qquad (5.9)$$

Again care has been taken when averaging (5.8) to avoid counting occupied states in dz^2 band.

At the absorption peak E_{vc}

$$\begin{aligned} a_1/a_3 &= |\langle \Psi_v | x | \Psi_c \rangle|^2 J(E_{vc}) / |\langle \Psi_v | z | \Psi_c \rangle|^2 J(E_{vc}) \\ &= 6.9/2.2 \approx 3 \end{aligned} \qquad (5.10)$$

which is in qualitative agreement with experiment.

Using the same program, we calculate the corresponding quantities for $NbSe_2$:

$$a_1/a_3=15/1.8\approx 8 \qquad (5.11)$$

In order to compare the results with experiment, we plot the calculated intensities as functions of the wavelength in FIGURE 6, assuming that the matrix elements are frequency-independent in the region under consideration.

To conclude we make the following points.

1) Assigning the optical experiment data to interband transitions has been a controversial subject for the TMD's. Different authors obtain different results based on different experiment or model[20,21,22], and little consistency has been achieved ,even within the results of the same author.

2) Bechthold et.al.[20] have assigned the transition at 2.7eV to dz^2-to-d/p transition. But we believe that this should be the p/d-to-dz^2 transition based on our calculation and the fact that this transition peak is strong in low frequencies and its position remains approximately unchanged after intercalation.

3) Usually people take it for granted that all transition matrix elements are approximately equal [21]. It turns out ,however,that when polarization is included , the relative magnitude of different matrix elements becomes important. In the case of single layer NbS_2 the matrix element of σ-

to-σ transition is about 7 times that of π-to-σ transition. Physically this means that the dipole moment parallel to layer is about 7 times that perpendicular to the layer. If one ignores the matrix element effect , he will not be able to understand why the σ-to-σ transition is stronger than π-to-σ transition based only on the joint density of states.

4) People have been applying the atomic selection rules in considering the interband transitions in TMD's[4,22] which is equivalent to the one center approximation we made in (5.6). But we believe that it is not well justified a priori. Thus the matrix elements we calculated is a crude estimation and the relative magnitude of the theorectical curves in FIGURE 6 is not very reliable.

VI. CONCLUSIONS

The statistical behavior of the single layer platelets suspended in water is understood in terms of a simple model of magnetically anisotropic single layers.

The qualitative agreement of this work with experiments supports the original band calculation of Wexler and Woolley[9]. Moreover the reduction of dimensionality can be acounted for by a tight binding model with zero interlayer interaction.

More work is needed to study the size distribution and light scattering and to calculate the interband matrix elements more accurately.

We hope this work will motivate the preparation of more single layer TMD's and initiate more sophisticated theories.

BIBLIOGRAPHY

[1] J.A.Wilson, F.J.diSalvo, and S. Mahajan, Adv. Phys. 24 , 117(1975)

[2] S.K. Chan, and V. Heine, J.Phys. F 3 , 795(1973)

[3] J.M.Rice and G.K.Scott, Phys. Rev. Lett. 35, 120(1975)

[4] C.Liu, O.Singh, P.Joesen, A.E.Curzon and R.F.Frindt, Thin Solid Films. 113 , 165(1984); See also C. Liu, M.Sc. Thesis, Simon Fraser University (1982)

[5] J.Tersoff and L.M.Falicov, Phys. Rev. B26, 6186(1982)

[6] N.J.Doran, B.Ricco, D.J.Titterington and G.Wexler,J.Phys.C, 11, 685(1978)

[7] J.A.Wilson and A.D.Yoffee, Adv. Phys. 18, 193(1969)

[8] W.H.de Jeu, Physical Properties of Liquid Crystalline Materials, New York: Gordon and Breach(1980)

[9] G.Wexler and A.M.Woolly, J. Phys.C, 9, 1185(1976)

[10] L.F.Matheiss, Phys. Rev. B5, 290(1972)

[11] N.J.Doran, B.Ricco, M.Schreiber, D.J.Titterington and G.Wexler, J. Phys. C, 11, 699(1978)

[12] J.C.Slater and G.F.Koster, Phys. Rev. 58, 1498(1954)

[13] A.H.McDonald, S.H.Vosko and P.T.Coleridge, J. Phys. C, 12 , 2991(1979)

[14] A.H.McDonald and D.J.W.Geldart, Phys. Rev. B24 ,469(1981)

[15] P.k.Misra and L.Kleiman, Phys. Rev. B5 ,4581(1972)

[16] Y.Yafet,Solid State Phys. 14, 1(1963)

[17] D.W. Murphy and G.W.Hull, Jr., J.Chem. Phys. 62 , 173(1975).

[18] S.J.Hillenius and R.V.Coleman, Phys.Rev. B18 ,3790(1978)

[19] C.Liu and R.F.Frindt(1984), to be buplished.

[20] P.S.Bechthold, R.Manzke and R.Schollhorn, J.Physique,Colloque C6 , 159(1984)

[21] W.Y.Liang and A.R.Beal, J.Phys.C, 9 , 2823(1976)

[22] S.S.P.Parkin and A.R.Beal, Phil. Mag. 42 , No.5, 627(1980)

APPENDIX A - FORMULATION OF THE MAGNETIC SUSCEPTBILITY

The theory of Misra and Kleinman[15] gives

$$\chi = -\ 0.5 g^2 \mu_B^2 f(En) \qquad (A.1)$$

where f(En) is the Fermi funtion, and En the energy, and

$$g^2 = -2\lambda^\alpha \lambda^\beta \mu_B^2 (L_\alpha + \tfrac{1}{2} g_s \sigma_\alpha)_{n\rho' n\rho} (L_\beta + \tfrac{1}{2} g_s \sigma_\beta)_{n\rho' n\rho} \qquad (A.2)$$

$$= \sum_{\alpha\beta} \lambda^\alpha G_{\alpha\beta} S'_\beta \qquad (A.3)$$

where α is the direction cosine of the magnetic field B and $S^\beta = (1/2)\sigma^\beta$ is the component of the Pauli matrice which is fixed with respect to rotation of the coordinate system. In our problem, we choose the coordinate system such that the components of the magnetic moment can be expressed in terms of the the corresponding coefficients of the Pauli matrices, and the G's are defined as follows[16]

$$- G\alpha x = 2\mathrm{Re}\langle \psi_{n\bar{k}\uparrow} | \mu_\alpha | \psi_{n\bar{k}\downarrow} \rangle$$

$$- G\alpha y = -2\mathrm{Im}\langle \psi_{n\bar{k}\uparrow} | \mu_\alpha | \psi_{n\bar{k}\downarrow} \rangle \qquad (A.4)$$

$$- G\alpha z = 2\langle \psi_{n\bar{k}\uparrow} | \mu_\alpha | \psi_{n\bar{k}\uparrow} \rangle$$

$$g^2(\bar{k}) = G\alpha x G\alpha x + G\alpha y G\alpha y + G\alpha z G\alpha z$$

$$= 4|\langle n+|\mu_\alpha|n+\rangle|^2 + 4|\langle n+|\mu_\alpha|n+\rangle|^2 \qquad (A.5)$$

for $\underline{B}$ along the $\vec{\alpha}$ direction
(A.5) is just the desired equation.

APPENDIX B - EVALUATION OF MATRIX ELEMENT OF TNE ORBITAL ANGLAR MOMENTUM

From the tight binding fit, one has ,using the same notation as (5.4),

$$|\psi\rangle = C_i|i\rangle \qquad (B.2)$$

and we need to consider dz^2 band only, as a first approximation.

One easily shows that

$$\begin{aligned} L_z|3\rangle &= 4|3\rangle \\ L_z|5\rangle &= 2|3\rangle \qquad (B.3) \\ L_z|i\rangle &= 0 \qquad (i \neq 3,5) \end{aligned}$$

Therefore

$$\langle\psi|L_z|\psi\rangle/\langle\psi|\psi\rangle = \sum_i (4C_i^* C_3 S_{i3} + C_i^* C_5 S_{i5}) / \sum_{ij} C_i C_j S_{ij} \qquad (B.4)$$

where S_{ij} is the overlap intergral. And

$$\langle\psi|L_x|\psi\rangle = 0 \qquad (B.5)$$

Because $L_x|i\rangle = |odd\rangle$

(B.4) and (B.5), together with Ci's and S_{ij}'s from the program, enable us to evaluate g^2 over the the Brillouin zone.

APPENDIX C - TETRAHEDRON METHOD IN TWO DIMENSION

The purpose is to evaluate the following in two dimension[13]:

$$J(E)=\int dk F(k)\theta(E-E(k))$$
$$I(E)=\int dk F(k)\delta(E-E(k)) \qquad (C.1)$$

where $I(E)=dJ(E)/dE$ is the electronic density of states.

We divide the Brillouin zone into triangles(microzones) as was shown in FIGURE 17(a), and we are able to write

$$J(E)=V_M \sum n^i \sum_{K=1}^{3} J_K^i F_K^i$$
$$I(E)=V_M \sum_i g^i \sum_K I_K^i F_K^i \qquad (C.2)$$

where V_M is the volume of the microzone, F_K^i is the F value at corner K of the ith microzone and E_K's have been arranged in ascending order. We have the folowing cases(see FIGURE 17(b) for one particular zone as an example)

(1) $E<E_1$

$g=0$

(2) $E_1<E<E_2$

Define $f_{nm}=(E-E_m)/(E_n-E_m)$

$n^i=f_{21}f_{31}$

$J_1=(1+f_{12}+f_{13})/3$

$J_2=f_{21}/3$

$J_3=f_{31}/3$

$g^i=2n^i/(E-E_1)$

$I_1^i=(f_{12}+f_{13})/2$

$I_K^i=f_{K1}/2 \qquad (K=2,3)$

(3) $E_2<E<E_3$

$n^i=(1-f_{13}f_{23})$

$J_1=(1-f_{13}^2 f_{23})/3n^i$

$J_2=(1-f_{23}^2 f_{13})/3n^i$

$J_3=[1-f_{13}f_{23}(1+f_{32}f_{31})]/3n^i$

$$g^{i}=2(1-n^{i})/(E_3-E)$$

$$I_K^{i}=f_{K3}/2 \qquad (K=1,2)$$

$$I_3^{i}=(f_{31}+f_{32})/2$$

(4) $E_3<E$

$$g=0$$

the above equations enable us to evaluate (4.1).

APPENDIX D - EVALUATION OF THE ATOMIC TRANSITION MATRIX

From TABLE 4. and the following equations

$$\cos Y = \sqrt{\frac{(\ell+m+1)(\ell-m+1)}{(2\ell+1)(2\ell+3)}}\,Y^{m}_{\ell+1} + \sqrt{\frac{(\ell+m)(\ell-m)}{(2\ell+1)(2\ell-1)}}\,Y^{m}_{\ell-1}$$

$$\sin Y = \left\{ -\sqrt{\frac{(\ell-m+1)(\ell-m+2)}{(2\ell+1)(2\ell+3)}}\,Y^{m-1}_{\ell+1} + \sqrt{\frac{(\ell+m)(\ell+m-1)}{(2\ell+1)(2\ell-1)}}\,Y^{m-1}_{\ell-1} \right\} e^{i\varphi} \quad \text{(D.1)}$$

we easily write

$$zY^{0}_{2} = \left(\sqrt{\frac{9}{35}}\,Y + \sqrt{\frac{4}{15}}\,Y \right) r$$

$$zY^{0}_{1} = \left(\sqrt{\frac{4}{15}}\,Y^{0}_{2} + \sqrt{\frac{1}{15}}\,Y^{0}_{0} \right) r$$

etc. (D.2)

Therefore there are three nonvanishing T^{z}_{ij}'s ($T^{z} = \langle odd | z | even \rangle$)

$T^{z}_{51} = \sqrt{4/15}$ $\quad T^{z}_{14} = \sqrt{1/15}$ $\quad T^{z}_{25} = \sqrt{1/5}$ (D.3)

Similarly we have for nonvanishing T^{x}_{ij}'s ($T^{x} = \langle even | x | even \rangle$)

$T^{x}_{52} = 1/2\sqrt{5}$	$T^{x}_{53} = 1/2\sqrt{5}$	$T^{x}_{41} = 1/\sqrt{15}$
$T^{x}_{42} = 1/2\sqrt{5}$	$T^{x}_{43} = 1/2\sqrt{5}$	$T^{x}_{14} = -1/2\sqrt{15}$
$T^{x}_{24} = -1/2\sqrt{5}$	$T^{x}_{34} = 1/2\sqrt{5}$	$T^{x}_{15} = -1/2\sqrt{5}$
$T^{x}_{25} = 1/2\sqrt{5}$	$T^{x}_{35} = -1/2\sqrt{5}$	(D.4)

FIGURE CAPTIONS

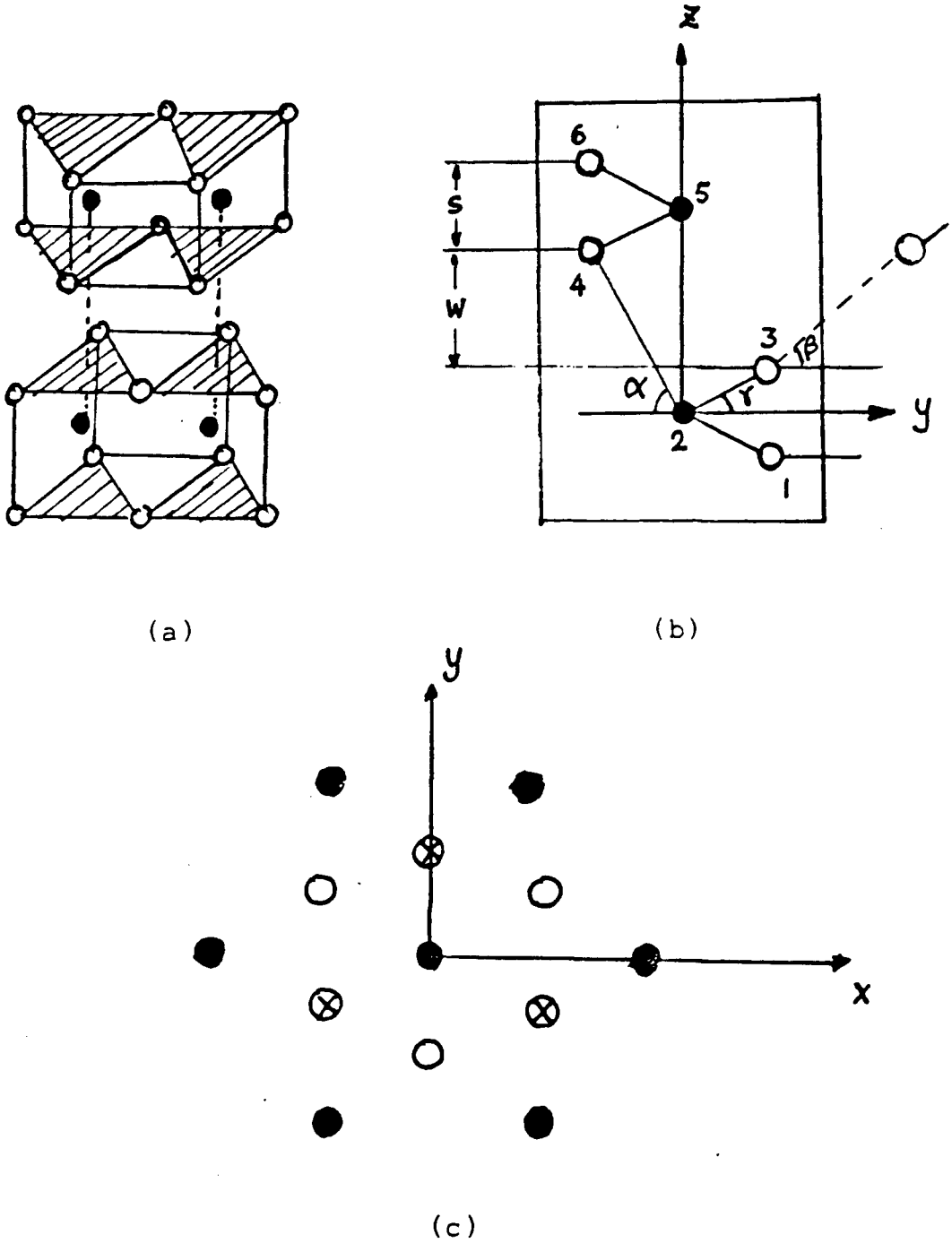

Figure 1 - Structure of 2H-TMD

(a) Structure of 2H-TMD(○ chalcogens, ● metal); (b) The Unit Cell of NbS_2; (c) The Strucure of NbS_2 looking down the c axis(⊗ S atoms in sandwich 1, ○ S atoms in sandwich 2).

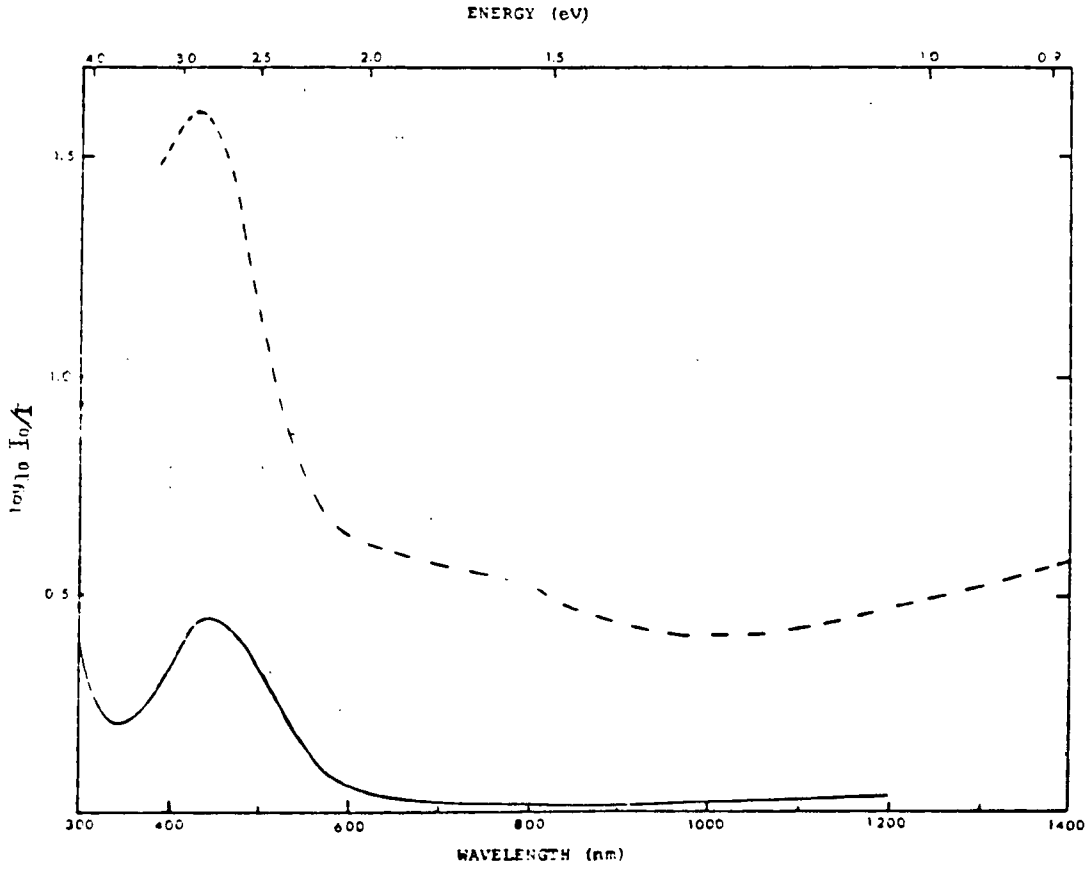

Figure 2 - Optical Absorption Spectra of NbS_2*

(——) Spetra of single layers; (---) Spectra of single crystal.

*Taken from ref. 4

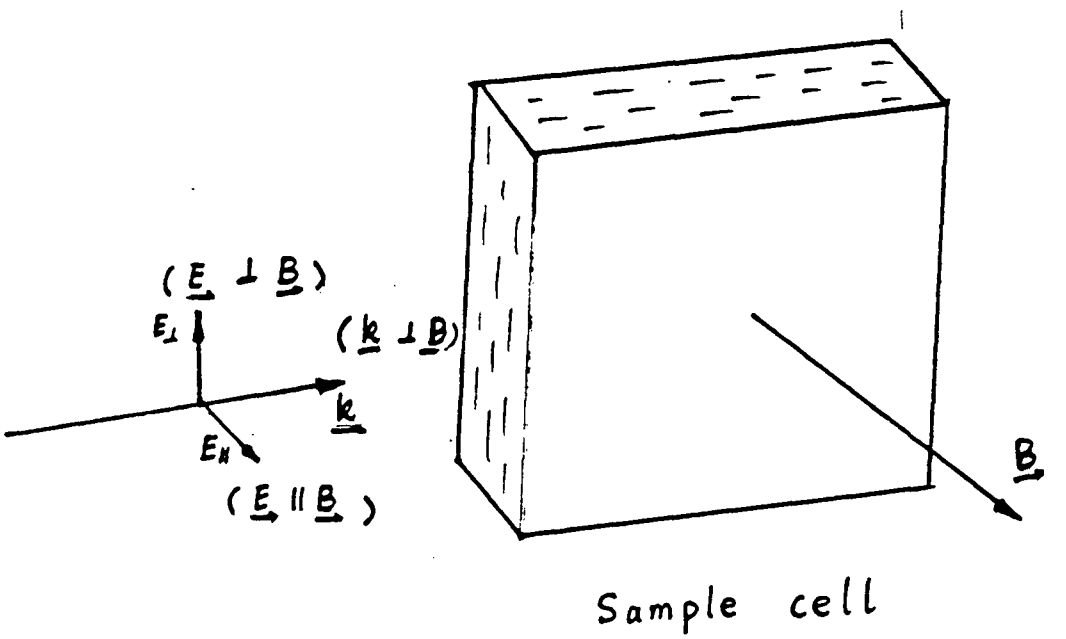

Figure 3 - The Aligment of NbS_2 Platelets in Magnectic Field

k is the wave vector of the incident light;

B is the applied magnetic field

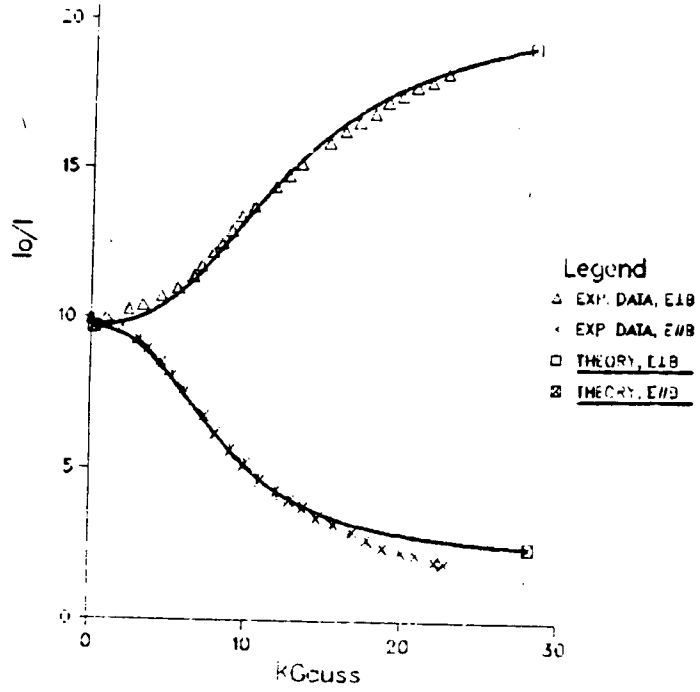

(a)

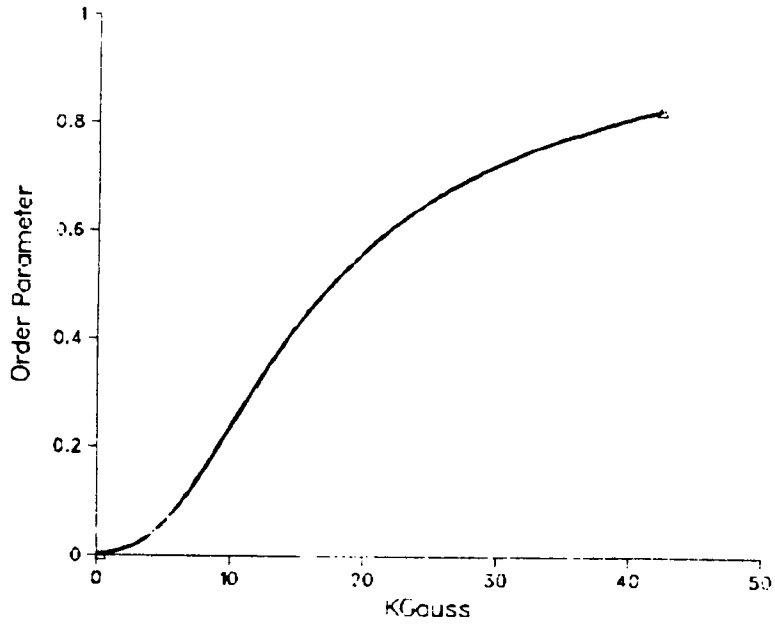

(b)

Figure 4 - Fitting of the Model to Experiment

(a) Fiting I_0/I to experiment in ref. 4. (b) The order parameter

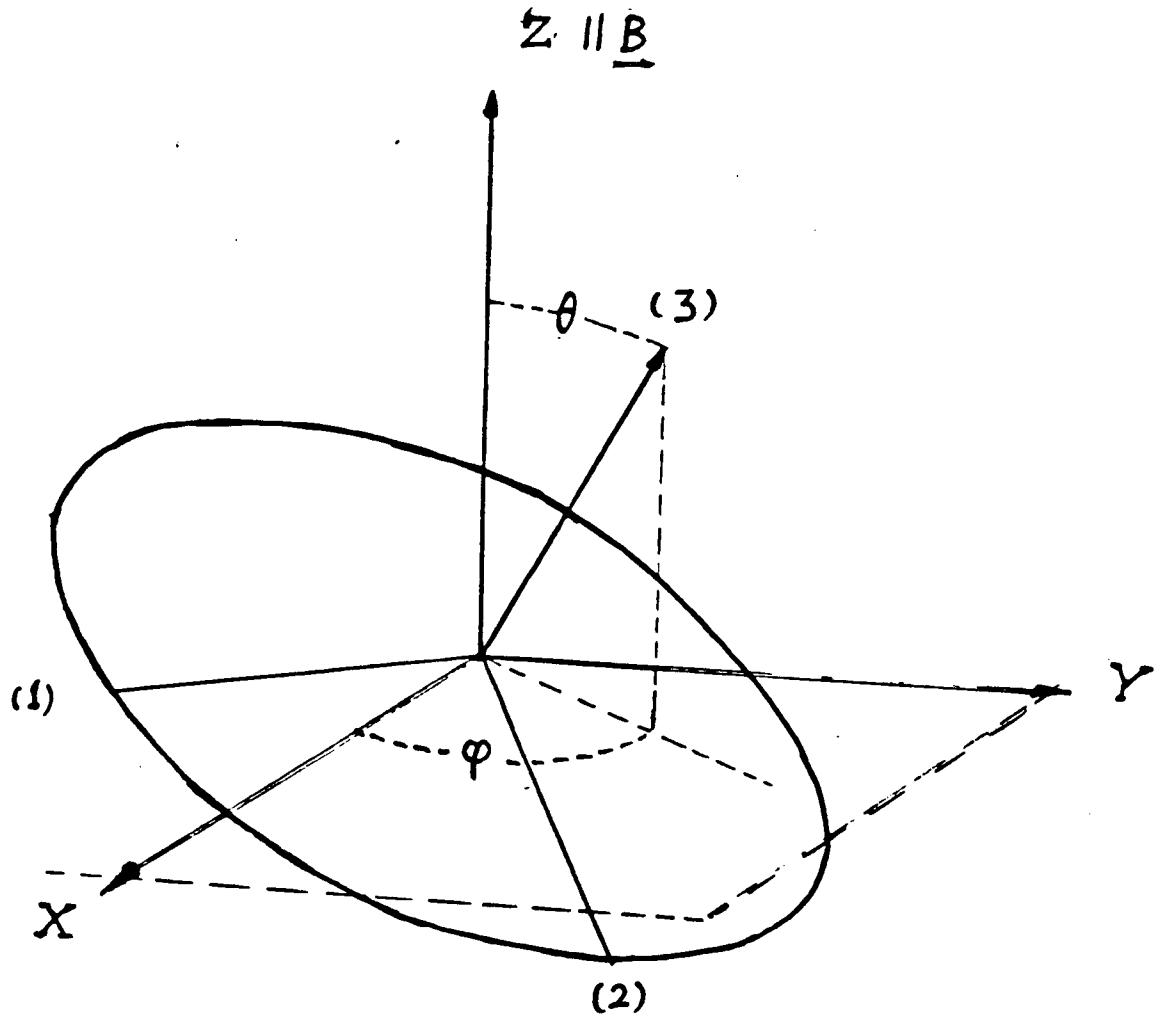

Figure 5 - Coordinates of the Single Layer

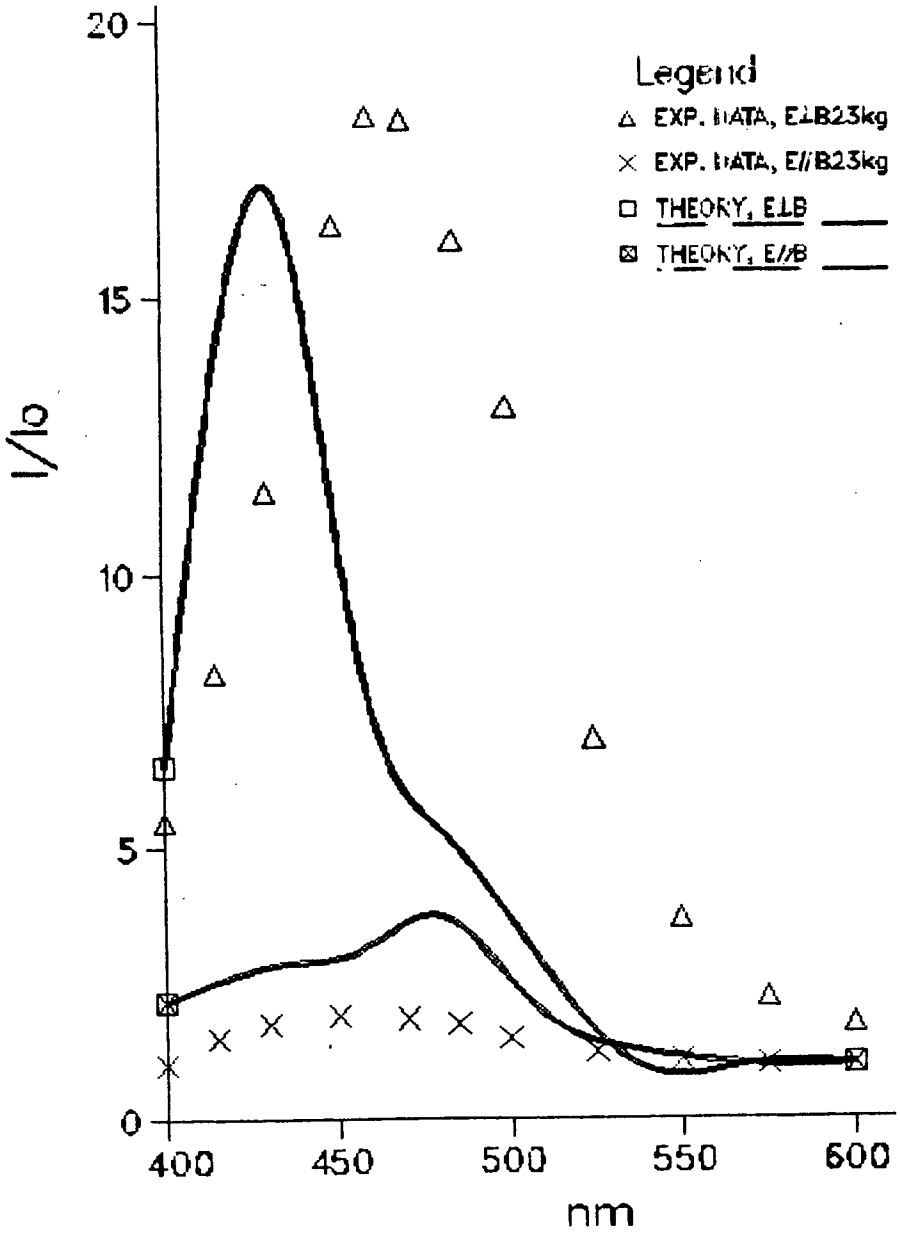

Figure 6 - Absorption spectra in Magnetic Field*
* Δ,X are digitized data points from ref. 4 , 19

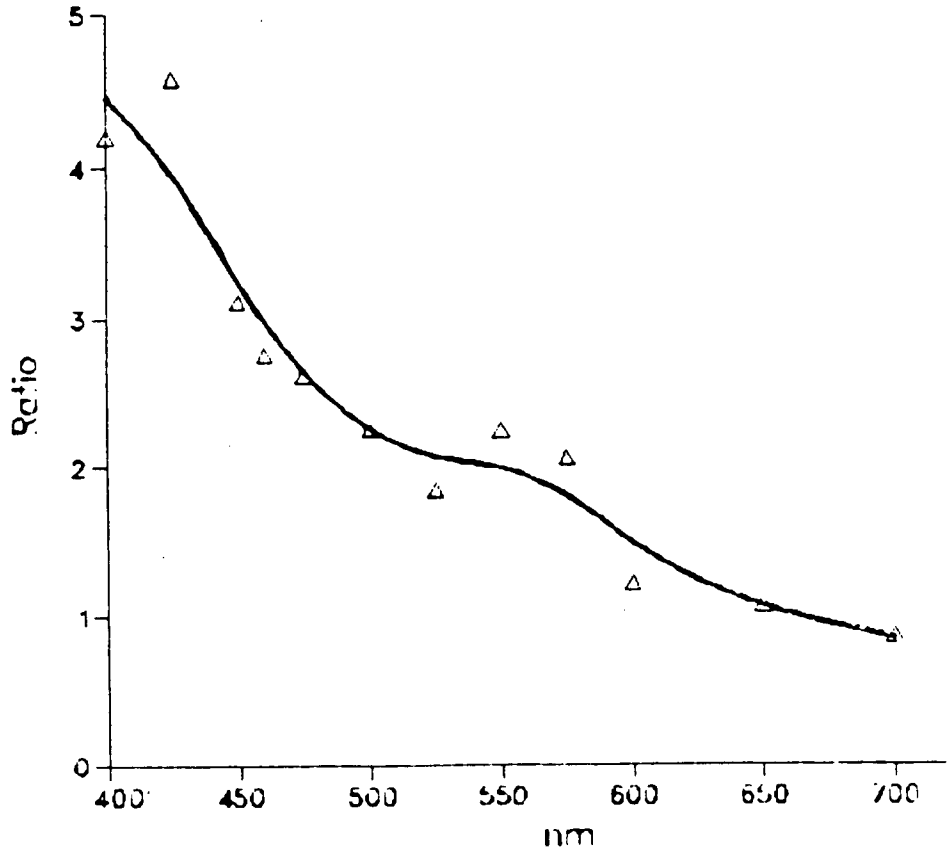

Figure 7 - Ratio of Intensities of Different Polariztions

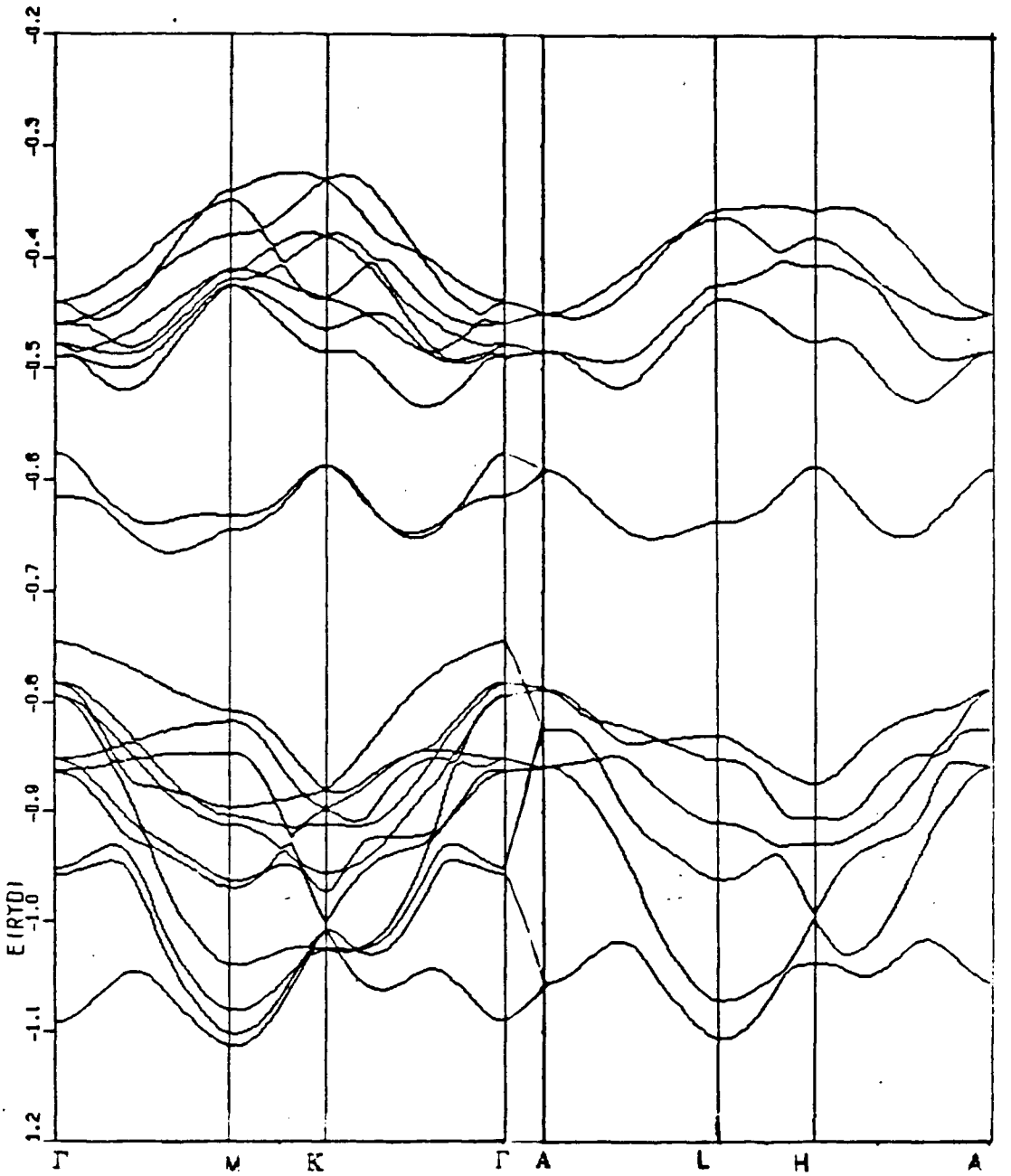

Figure 8 - Band Structure of $2H\text{-}NbS_2$

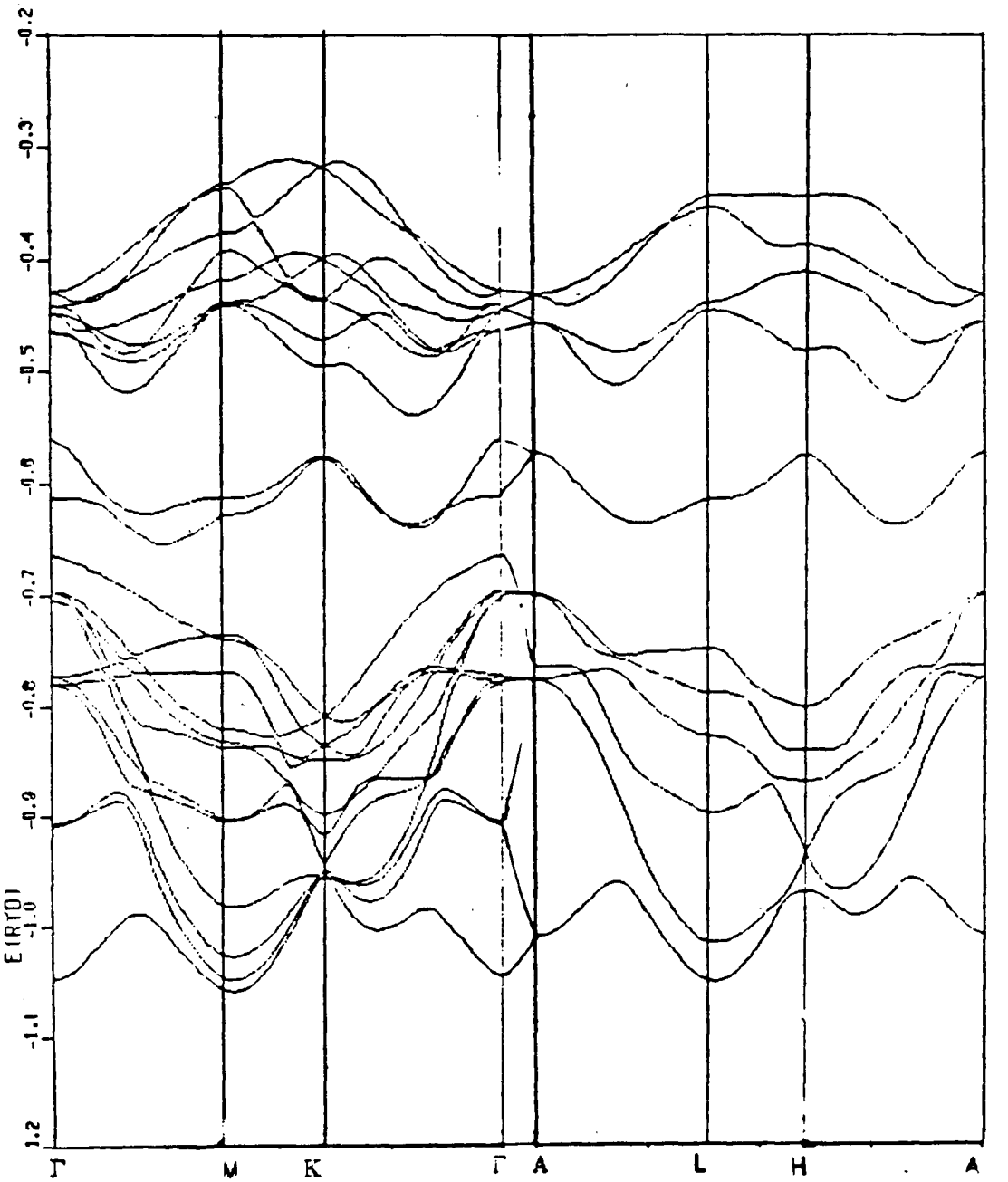

Figure 9 - Band Structure of 2H-$NbSe_2$

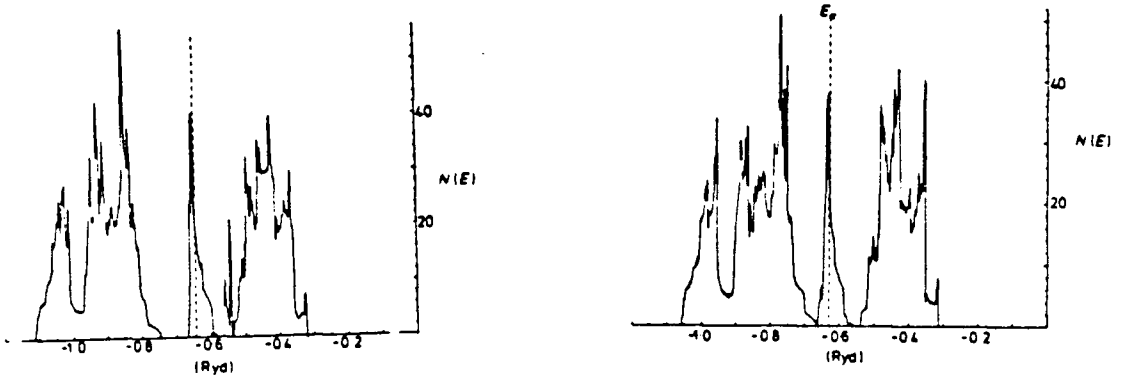

(a) (b)

Figure 10 - Density of States of the 3D Compounds
(a) DOS of NbS_2; (b) DOS of $NbSe_2$

in unit of 1/(Nb.spin.Ryd)

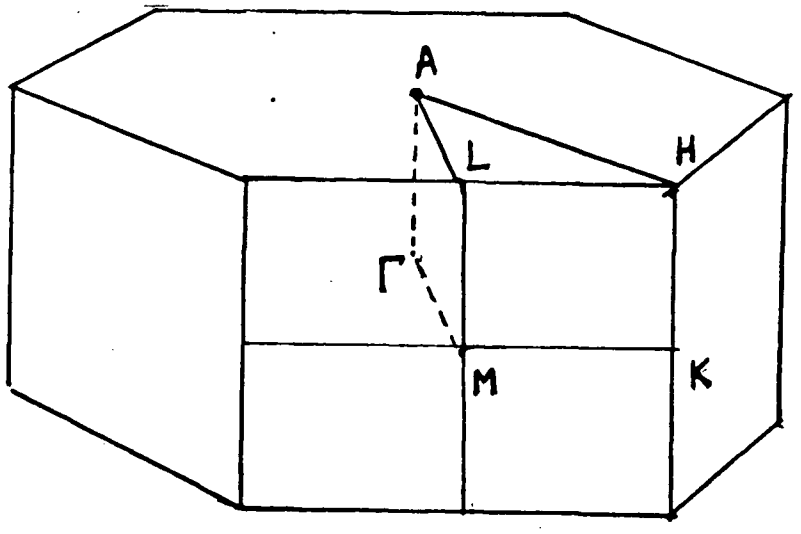

Figure 11 - Symmetry Points in the Brillouin Zone

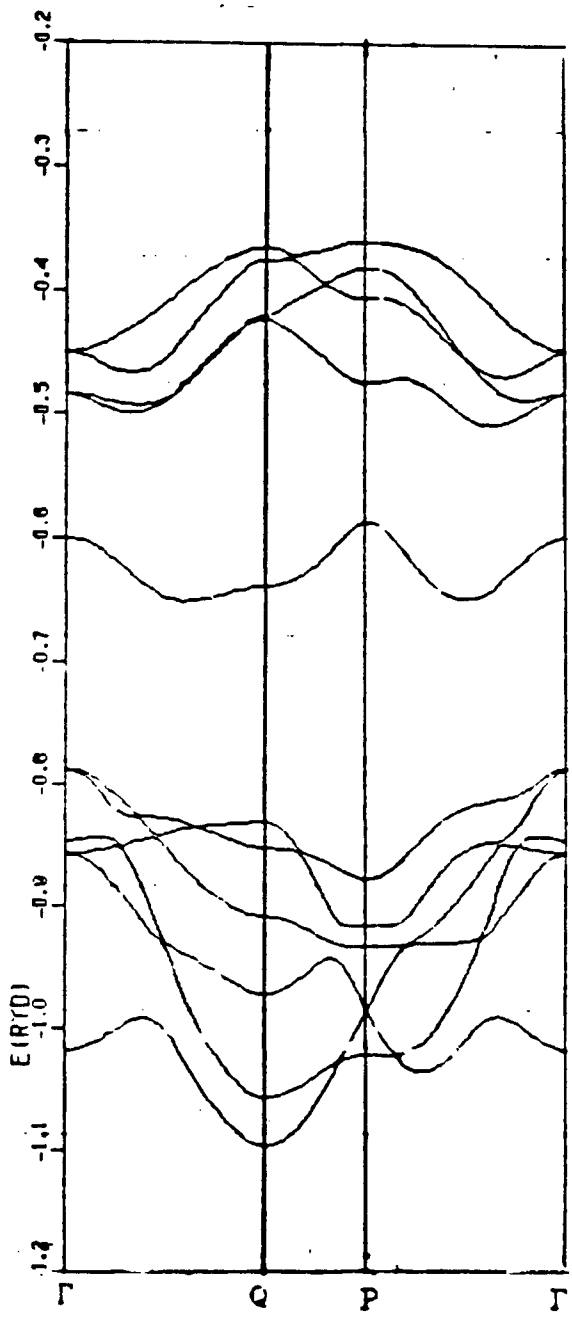

Figure 12 - Band Structure of Single Layer NbS_2

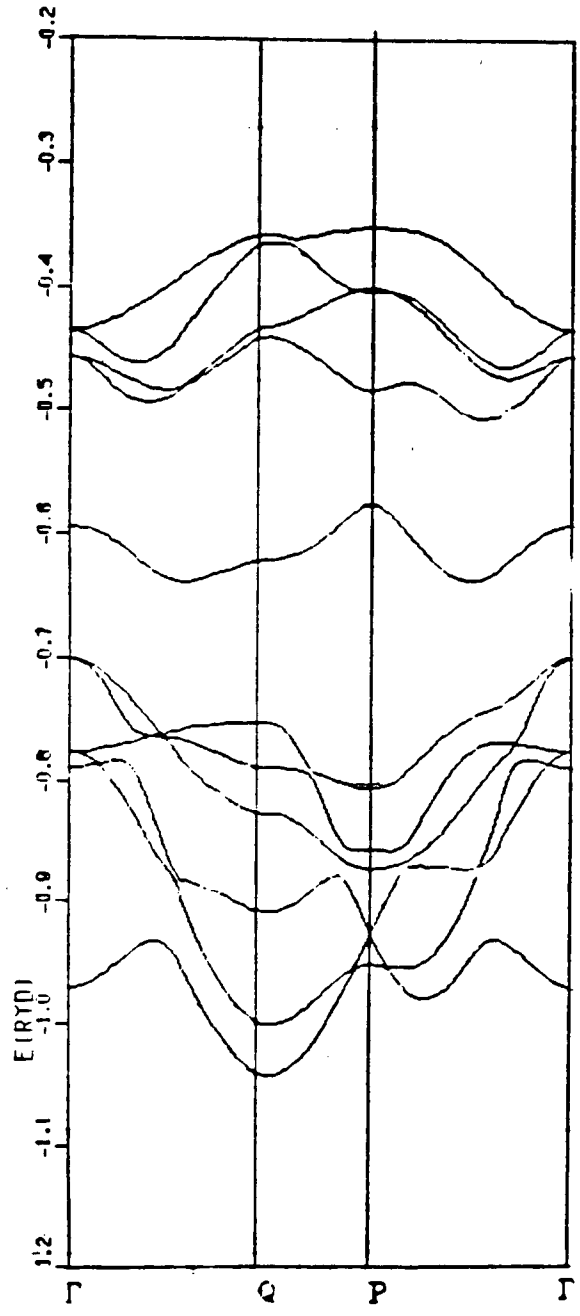

Figure 13 - Band Structure of Single Layer $NbSe_2$

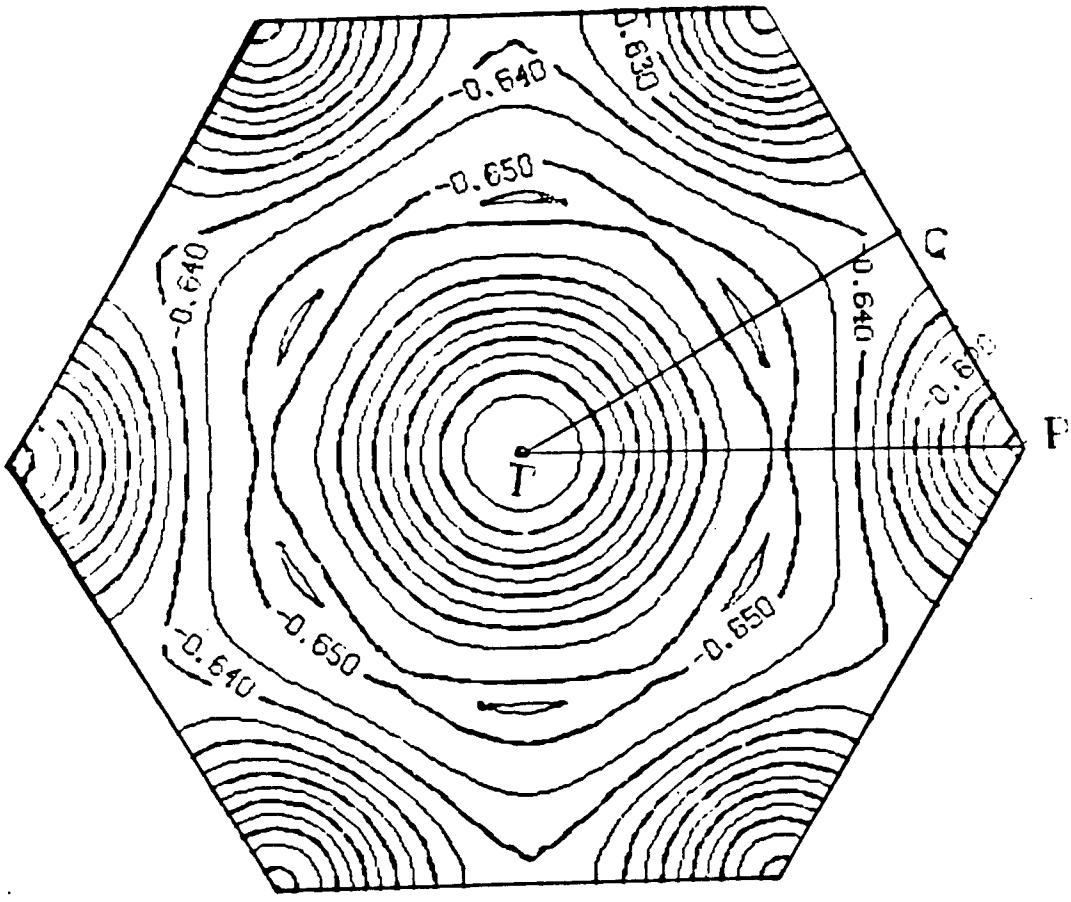

Figure 14 - Fermi Surface of Single Layer NbS_2
Fermi Energy=-0.64 Ryd

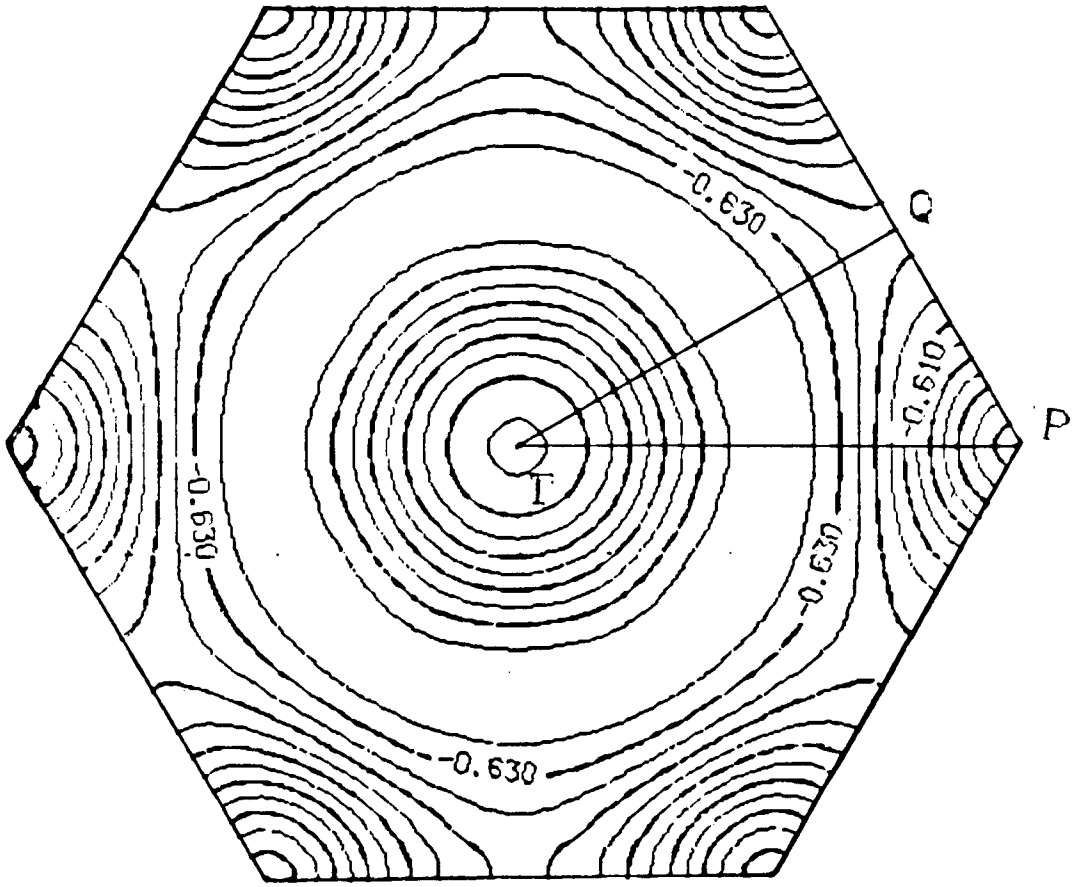

Figure 15 - Fermi Surface of Single Layer $NbSe_2$
Fermi Energy=-0.635 Ryd

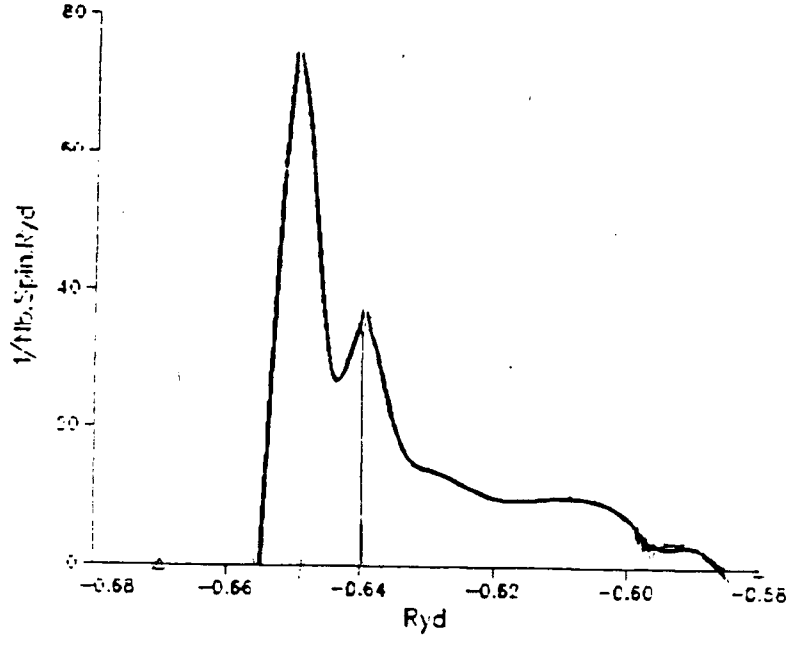

(a)

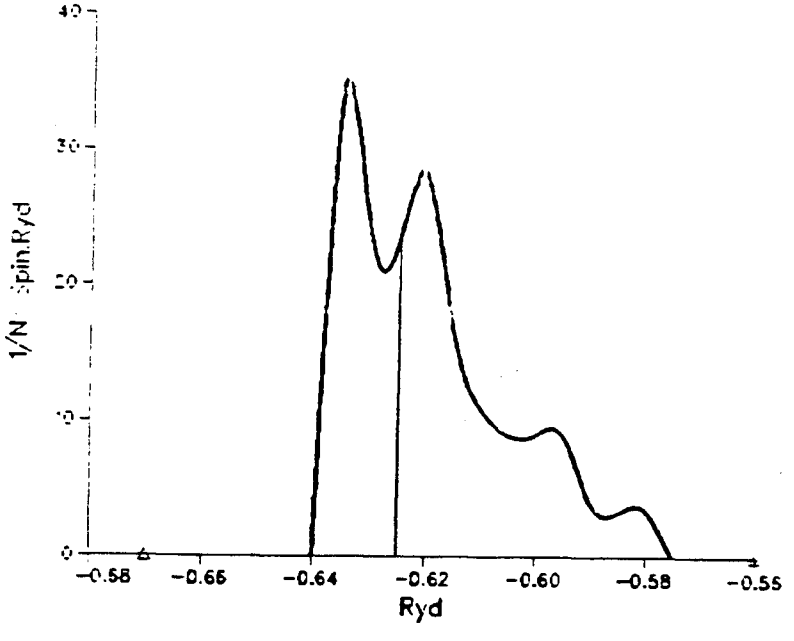

(b)

Figure 16 - Density of States(dZ^2) of the Single Layers (a) DOS of NbS_2; (b) DOS of $NbSe_2$, in unit of 1/(Nb.Spin.Ryd)

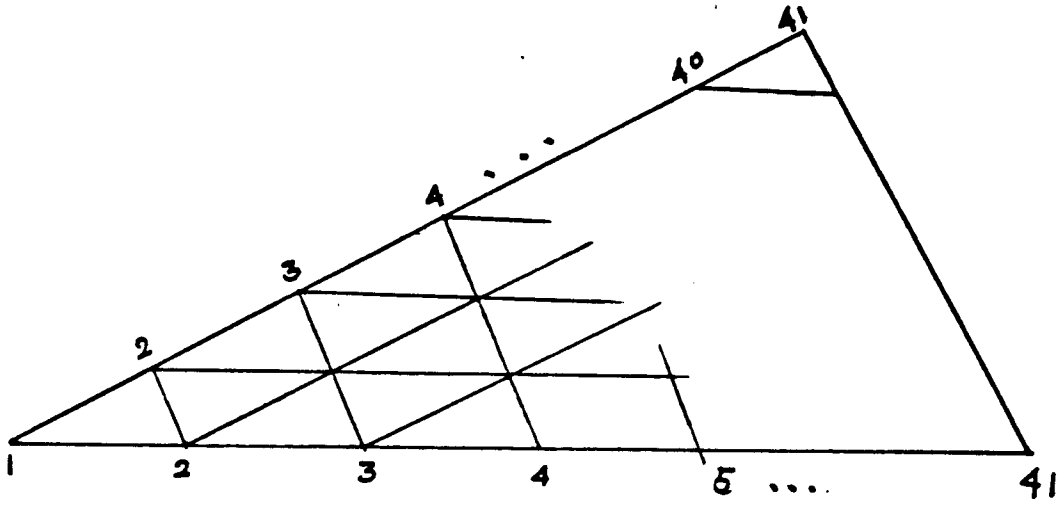

(a)

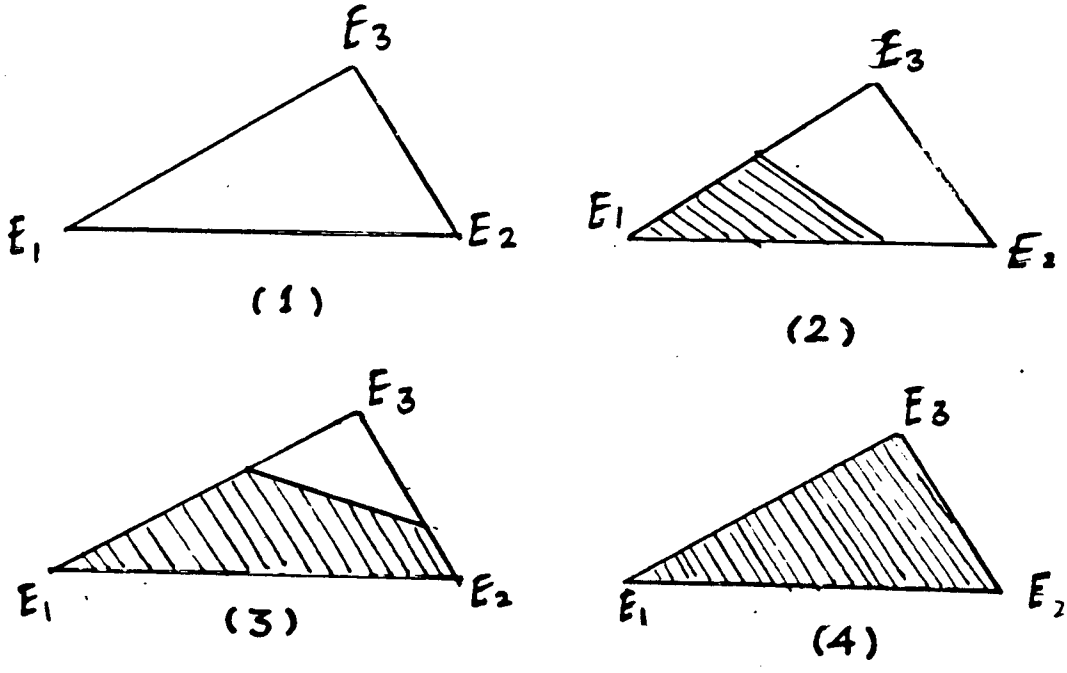

(b)

Figure 17 - Diagram Illustrating the Tetrahedron Method

(a) Brillouin zone grid; (b) Diagram of the four cases.

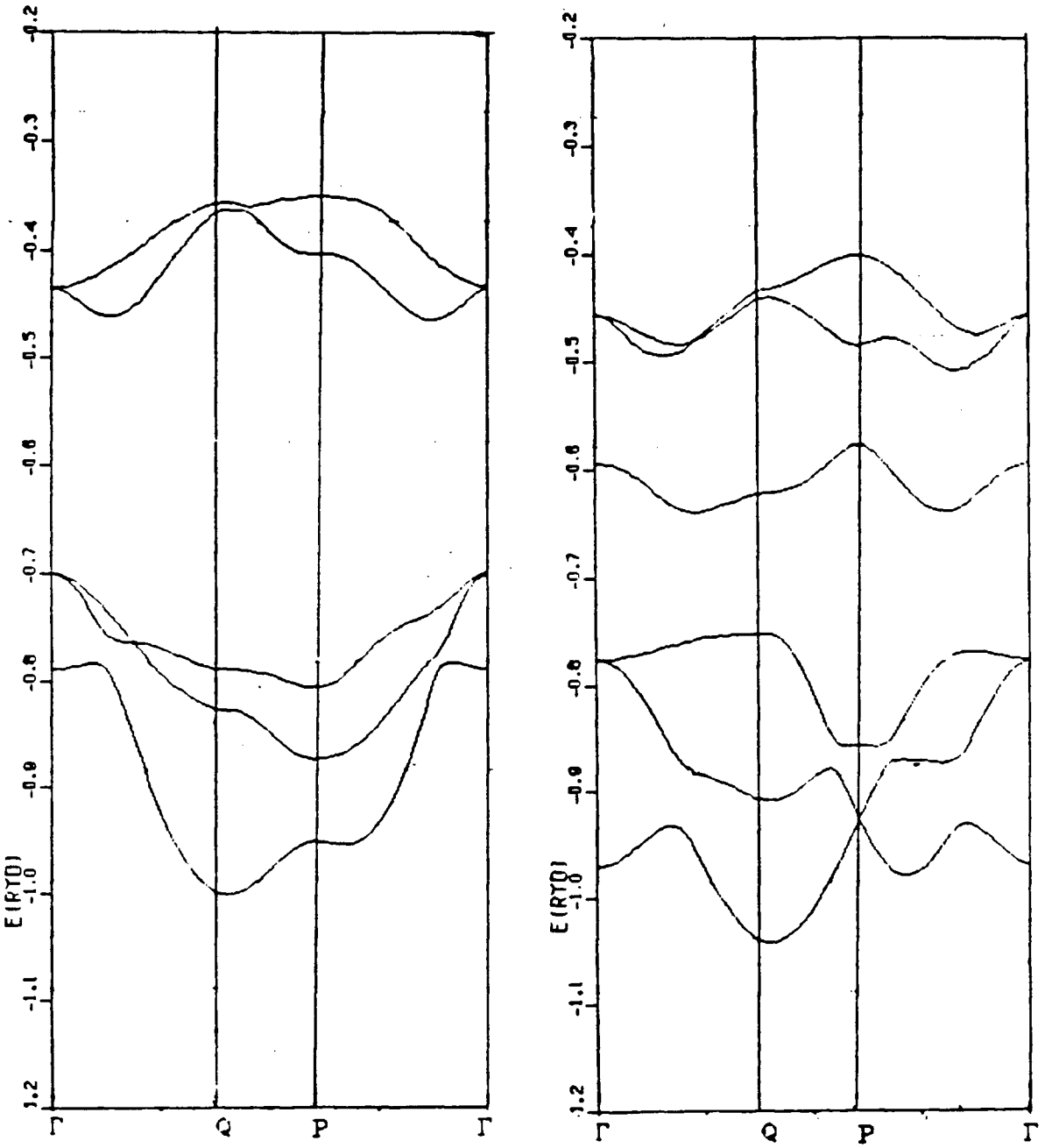

(π) (σ)

Figure 18 - Separation of Bands of the Single Layer NbS_2

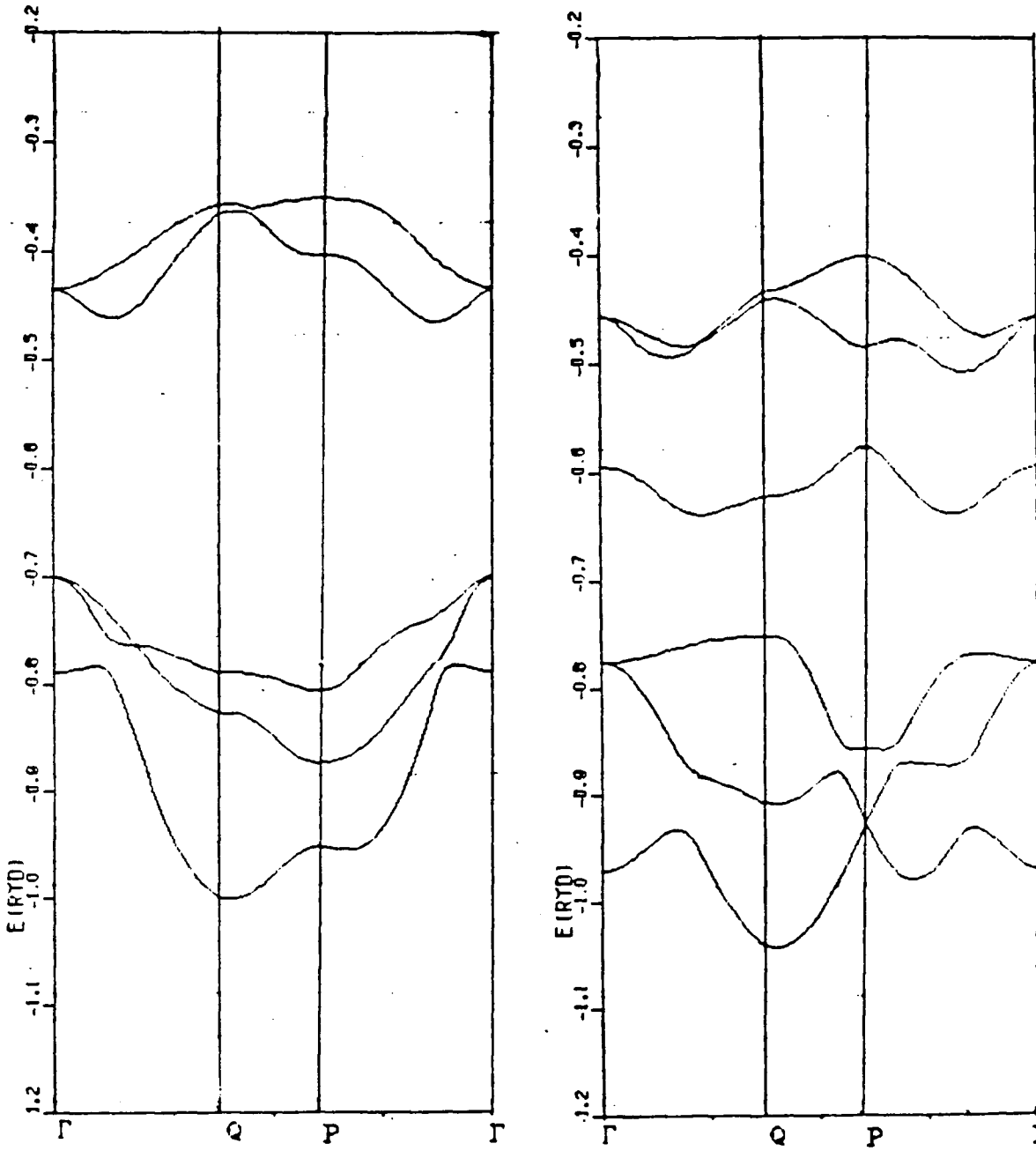

(π) (σ)

Figure 19 - Separation of Bands of the Single Layer $NbSe_2$

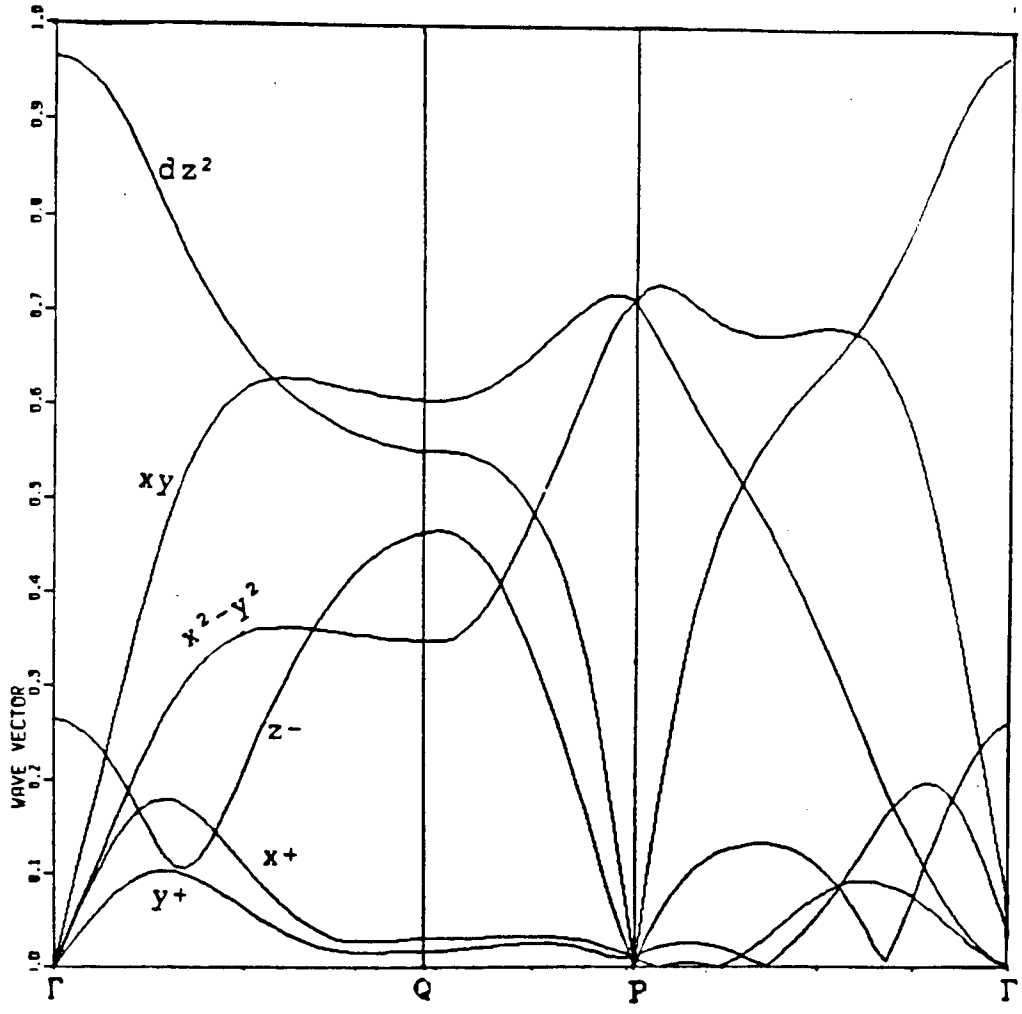

Figure 20 - Amplititude Coefficients of the Wave Funtion for dz^2 Band

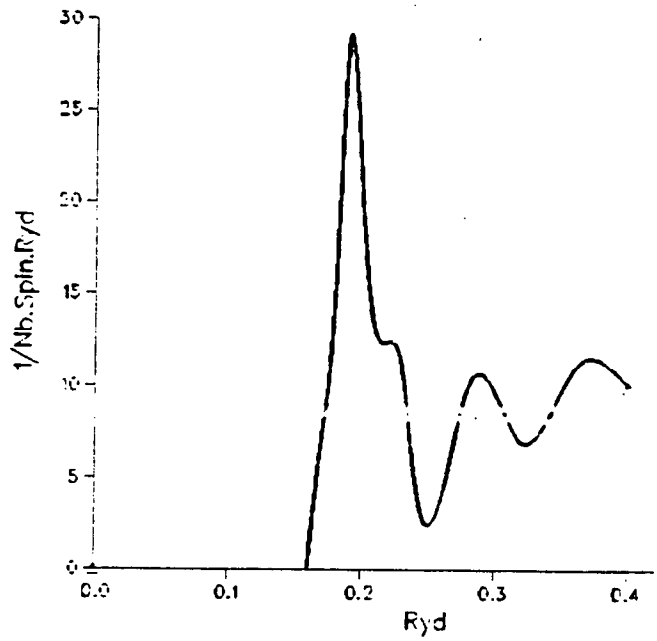

(a)

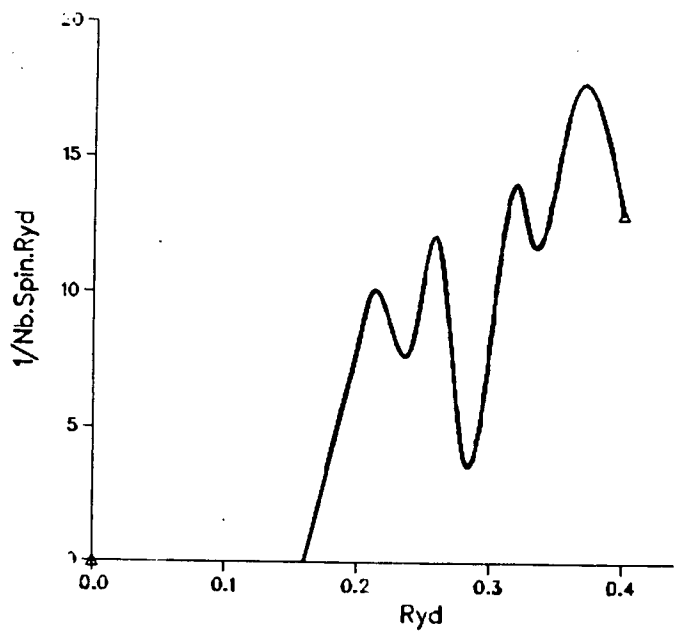

(b)

Figure 21 - Joint Density of States of Single Layer NbS_2
(a) π to σ transtions; (b) σ to σ transtions.

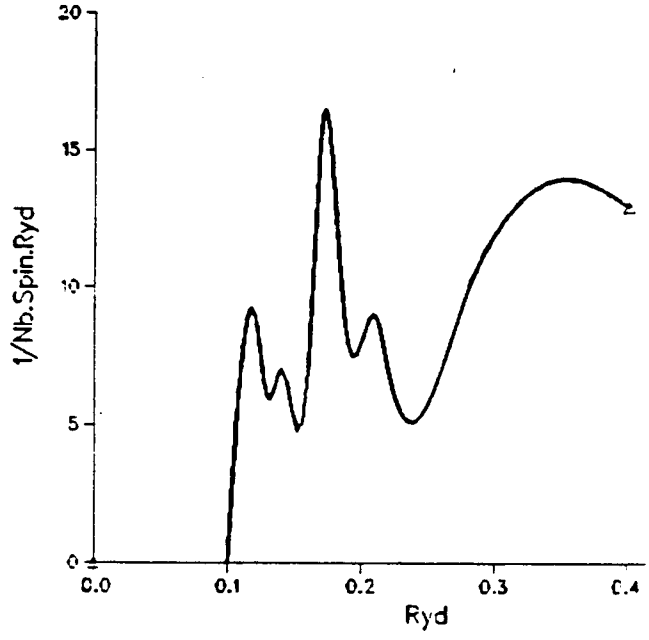

(a)

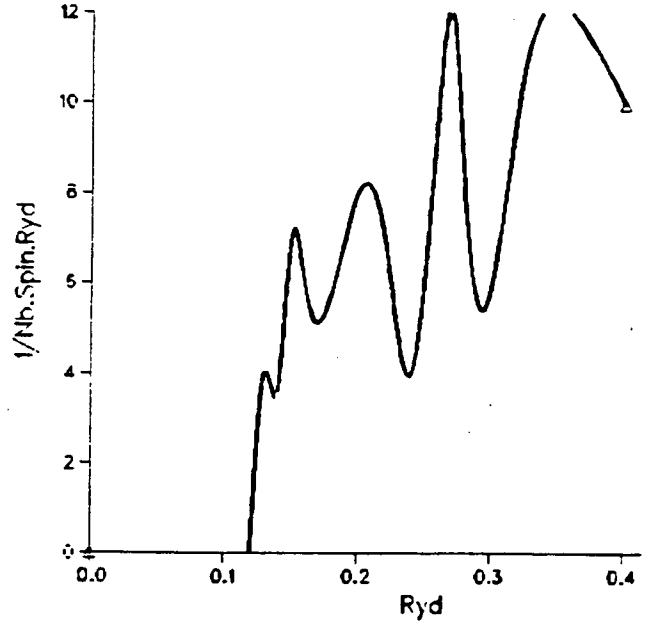

(b)

Figure 22 - Joint Density of States of Single Layer $NbSe_2$
(a) π to transtions; (b) σ to σ transtions.